Engineering Structures 189 (2019) 523–540

Contents lists available at ScienceDirect

Engineering Structures

journal homepage: www.elsevier.com/locate/engstruct

Experimental investigation on the influence of the aspect ratio on the in-plane/out-of-plane interaction for masonry infills in RC frames

Maria Teresa De Risi[1], Mariano Di Domenico*, Paolo Ricci, Gerardo Mario Verderame, Gaetano Manfredi

Department of Structures for Engineering and Architecture, University of Naples Federico II, Via Claudio 21, 80125 Naples, Italy

ARTICLE INFO

Keywords:
RC building
Infill masonry wall
Experimental test
Out-of-plane strength
In-plane/out-of-plane interaction
Aspect ratio

ABSTRACT

The analysis of the behaviour of masonry infills under out-of-plane (OOP) and in-plane (IP) loading is paramount to correctly assess the seismic performance of reinforced concrete (RC) frames. A very important issue about this topic is certainly the IP/OOP interaction, namely the analysis of how the IP damage, which affects infills during earthquakes, can influence their OOP behaviour (and vice-versa). Some studies about this topic were developed in the last years; nevertheless, only a dozen of tests currently exists in the literature to experimentally explore this key issue.

This work first presents an experimental campaign carried out on square infill walls in RC frames to investigate about the OOP behaviour of the masonry infills, and about the IP/OOP interaction. On the whole, four specimens have been tested under OOP monotonic loading. Three of them have been first damaged under cyclic IP actions, with different extent; the remaining one, used as a reference, was tested under OOP loading only. The experimental campaign is described in detail in terms of specimens' characteristics, material properties, adopted setup and instrumentation layout. The experimental results are analysed in terms of IP and OOP force-displacement responses, vertical arch strength contribution evolutions, and damage state evolutions, and compared with prediction proposals from the literature.

Then, the influence of the infill aspect ratio (width (w)-to-height (h) ratio) on the IP/OOP interaction is investigated by means of the comparison between data presented herein (collected on infills with w/h = 1) and a companion experimental campaign previously performed on nominally identical infills except that for the aspect ratio of the specimens (in that case, higher than the unit). It has been observed that under given IP drift levels, square infills presented lower IP damage levels with respect to rectangular infills (with w/h > 1), thus generally producing a less pronounced detrimental effect of the IP imposed drift on the OOP strength. Nevertheless, none of the predictions from literature takes into account the role of the aspect ratio on the IP/OOP interaction, generally resulting in conservative predictions, to be improved in future works.

1. Introduction

In present years, it is commonly recognized by the engineering community – and considered in modern building codes – that the seismic assessment and safety check of buildings cannot be considered exhaustive if non-structural elements' response, their contribution to buildings' seismic performance, and – above all – the risk related to their collapse are neglected. For this reason, current research is deeply focused on this topic. In the wide and heterogeneous world of non-structural elements, infill walls are certainly the most studied, as they contribute in the most significant way to structures' overall response and given that their damage and/or collapse is associated with significant repair/refurbishment costs and threat to human life.

Infill walls are interested by both in-plane (IP) seismic displacement demand and out-of-plane (OOP) seismic acceleration demand. IP and OOP responses are not independent, as the IP damage due to displacement demands influences the OOP response and vice-versa. This phenomenon is named "IP/OOP interaction".

The investigation of this issue was deepened in 90s through fundamental experimental and theoretical works. Dawe and Seah [1]

* Corresponding author.
E-mail addresses: mariateresa.derisi@unina.it (M.T. De Risi), mariano.didomenico@unina.it (M. Di Domenico), paolo.ricci@unina.it (P. Ricci), verderam@unina.it (G.M. Verderame), gamanfre@unina.it (G. Manfredi).
[1] Beneficiary of an AXA Research Fund postdoctoral grant.

https://doi.org/10.1016/j.engstruct.2019.03.111
Received 15 September 2018; Received in revised form 27 March 2019; Accepted 28 March 2019

tested unreinforced masonry (URM) infills in steel frames and proposed a mechanical-based OOP response model which is deeply discussed and analysed in Verderame et al. [2]. Angel et al. [3], tested URM infills in Reinforced Concrete (RC) frames and proposed a mechanical-based strength model for them accounting for the IP/OOP interaction effects. Bashandy et al. [4] proposed a mechanical-based out-of-plane strength formulation for URM infills in which two-way arching occurs. Flanagan and Bennett [5,6] tested URM infills in steel frames and proposed an empirical formulation for the prediction of their out-of-plane strength. Calvi and Bolognini [7] tested unreinforced and reinforced masonry infills in RC frames with both pure OOP and combined IP/OOP tests. A similar experimental campaign was performed by Pereira et al. [8].

In very recent years, experimental and numerical research on this topic was resumed. Kadysiewski and Mosalam [9] and Mosalam and Günay [10] proposed a fiber model for modelling the OOP response and collapse of URM infills and the IP/OOP interaction effects. A modified version of this modelling strategy was applied for the seismic assessment of RC frames by Longo et al. [11]. Varela-Rivera et al. [12] tested URM infills in RC frames. Agnihotri et al. [13] validated a 3D Finite Element Model (FEM) of Dawe and Seah [1]'s specimens and used such a model to discuss the influence of geometrical and mechanical parameters on the IP/OOP interaction effects. A similar numerical research was proposed by Mohyeddin et al. [14]. Guidi et al. [15] tested thin and thick unreinforced and reinforced masonry infills in RC frames with combined IP/OOP tests. Hak et al. [16] tested thick URM infills in RC frames with both pure OOP and combined IP/OOP tests. Furtado et al. [17,18] tested thin URM infills in RC frames with both pure OOP and combined IP/OOP tests and applied a simplified version of Kadysiewski and Mosalam [9]'s model for the seismic assessment of RC buildings. Alternative IP/OOP modelling strategy were proposed by Oliaee and Magenes [19], by Di Trapani et al. [20] and by Ricci et al. [21]. A detailed state of the art review of OOP strength models was proposed by Pasca et al. [22]. Di Domenico et al. [23] and Ricci et al. [24,25] performed pure OOP tests on infills with different slenderness and boundary conditions as well as combined IP/OOP tests of infills with different slenderness ratio.

Ongoing research is mainly focused on the design and experimental assessment of engineered infill walls characterized by the application of innovative solution for limiting the IP damage and ensure safety with respect to OOP actions (e.g., [26–28]).

Based on these studies, together with the results of previous experimental tests performed in the literature, the effectiveness of literature strength and displacement capacity models has been assessed and empirical formulations for modelling the OOP strength and stiffness reduction due to IP-damage have been proposed. However, some open issues still remain, both on the pure OOP behaviour and on the effects of the IP/OOP interaction.

The influence of vertical slenderness ratio (h/t) on the IP/OOP interaction effects was recognized first by Angel et al. [3]. This is strongly related to the influence of the h/t slenderness ratio on the entity of IP damage. In fact, as also discussed by Morandi et al. [28], at equal IP drift a higher damage level is expected for slender infills; hence, at equal IP drift, a higher OOP strength/stiffness reduction is expected for slender infills [25]. However, the IP response of infills is conditioned by the infill aspect (width-to-height, w/h) ratio, too. Hence, the IP damage due to IP actions could be influenced by the infill aspect ratio w/h. Therefore the infill aspect ratio w/h may have some effects on the entity of IP/OOP interaction effects. Only the numerical study by Agnihotri et al. [13] discussed this issue, which has never been checked through experimental tests.

Consider also that the database of URM infills in RC frames tested for the investigation of the IP/OOP interaction is yet very small (despite the fact that the ongoing research is contributing to rapidly enrich it) as it is currently constituted by around a dozen of tests [25]. A contribution to the enrichment of the database is still needed to improve the knowledge level on the OOP behaviour of infills and the IP/OOP interaction effects. Note also that the current experimental database is constituted, for what concerns infills in RC frames, only by results on rectangular infills.

In this paper, the results of four experimental tests on square URM infill walls realized with clay hollow bricks in RC frames (one pure OOP test and three OOP tests performed after IP tests carried out up to three different drift levels) are presented. The main issues investigated are the OOP strength of the IP-undamaged specimen, its reduction due to the effects of the IP damage and the effect of the infill aspect ratio, i.e., the width (w)-to-height (h) ratio, on the abovementioned reduction by means of the comparison with the results of analogous tests carried out on rectangular ($w/h > 1$) infills (previously presented in [24]).

The experimental results are presented with the support of IP and OOP force-displacement response diagrams together with the representation of damage and cracking patterns' evolution and of the evolution of the specimens' OOP deformed shape. The observed values of the IP-undamaged specimen strength is compared with the predictions of the available literature models. The results of the IP/OOP tests in terms of OOP strength reduction at different IP drifts are then compared with the prediction of literature formulations and some considerations on the influence of the specimens' unit aspect ratio on the effects of the IP/OOP interaction are presented and discussed.

2. Description of the experimental campaign

The experimental campaign is described in this section. Four specimens have been designed, realised and tested. One of them has been used as a reference and, therefore, it has been tested under out-of-plane loading only. The remaining three specimens were first damaged under in-plane actions – with three different IP damage levels (as in the corresponding experimental campaign on rectangular walls by Ricci et al. [24]) – and, then, tested under out-of-plane loading.

First, details about the geometrical and reinforcement properties of the RC frames and material properties are shown and commented in Sections 2.1 and 2.2. Then, Section 2.3 reports details about the loading setup adopted to perform the experimental tests and the instrumentation system used to monitor the responses of the specimens.

2.1. Specimens layout and details

The tested specimens are 1-bay-1-storey RC frames (see Fig. 1), designed according to the Italian seismic code [29], nominally identical for geometry and reinforcement details, with $200 \times 270\,mm^2$ columns. The upper beam has the same cross-section of the columns. The foundation beam has a $400 \times 400\,mm^2$ cross-section. The design of the concrete members was performed according to the strength hierarchy rules in agreement with the Italian seismic code mentioned before. As a result, a weak-beam-strong-column hierarchy is obtained, and shear failures of members and joints are prevented by means of a proper stirrups amount (see Fig. 1).

Each frame was filled with a masonry panel. The infill panel was built in total connection with the concrete frame along the four edges through mortar. Infill walls' thickness (t) is equal to 80 mm, realized with $250 \times 250 \times 80\,mm^3$ clay hollow bricks with a nominal void percentage equal to 60%, and 1 cm thick horizontal and vertical mortar joints. The clay hollow bricks were placed with the holes in the horizontal direction.

All the specimens were 2:3-scaled frames due to capacity limits of the laboratory equipment. It is worth noting that, in case of scaled specimens, some experimental works from literature found how (see e.g. [30,31]) the unit-to-wall size ratio could potentially influence the experimental response of unreinforced masonry walls, particularly referring to higher in-plane drift capacity and, consequently, out-of-plane response. Nevertheless, these studies were related to unreinforced masonry walls instead of masonry infills with a surrounding RC frame. Specific experimental campaign should be dedicated in future research

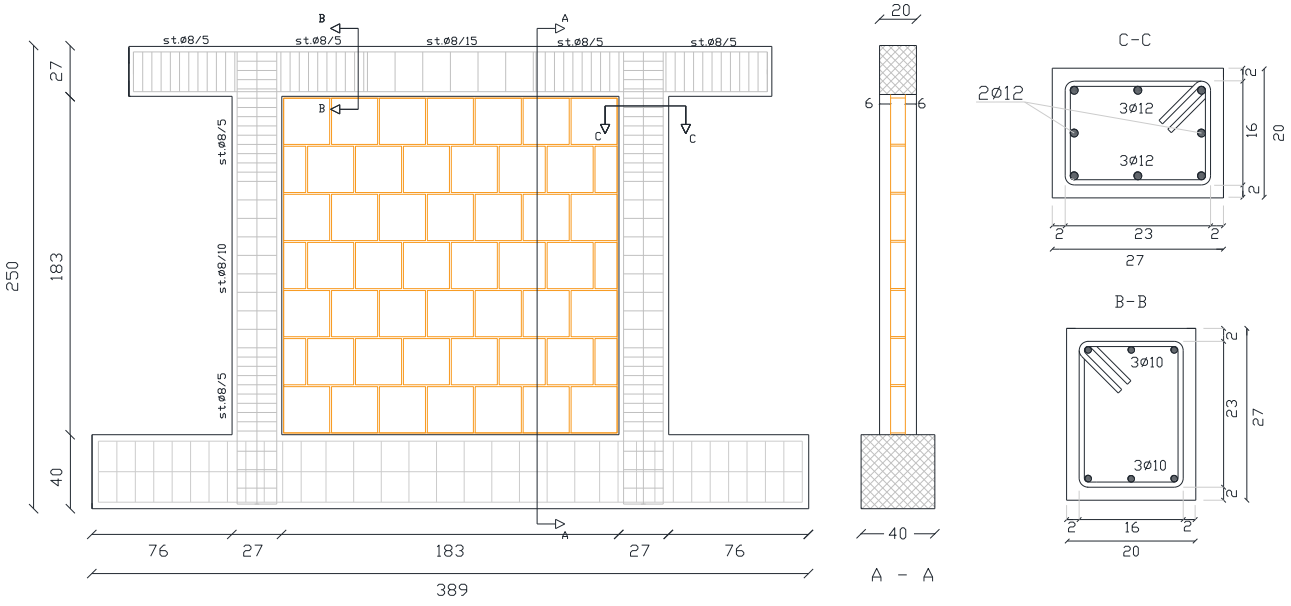

Fig. 1. Geometrical and reinforcement details of the tested specimens (dimensions are in cm).

works to investigate about such an influence on unreinforced masonry walls also at low drift level. Based on these remarks, and since the adopted scale factor is quite close to the unity, it can be argued that the possible influence of the size effect on the infills response, if any, should be at least mitigated in the experimental campaign described herein.

2.2. Material properties

The RC elements of the frames are characterized by a C32/40 class of concrete. Cylindrical mean compression concrete strength (f_c) has been determined by testing, according to the European standard EN 206-1 [32], 150 × 150 × 150 mm^3 cubic samples (by multiplying the mean cubic strength per 0.83, according to the Italian standard [29], resulting equal to 42.9 MPa (see Table 1). Longitudinal and transverse rebars are characterized by a B450C steel typology, with a nominal yielding strength equal to 450 MPa. Mean steel yielding (f_y) and ultimate (f_t) strength were evaluated by means of tensile tests carried out according to the European standard [33]. Both properties resulted dependent on the bar diameter, as shown in Table 1. Mechanical properties reported in Table 1 are mean values obtained by three specimens each. More specifically, three tensile tests on three samples were performed for each bar diameter. The related Coefficients of Variation (CoV) are also shown in the same table.

The mortar adopted for the infills is a nominally class M5 cementitious mortar. Compressive tests on mortar have been performed according to ASTM C109/C109M-16a [34] standard. Three mortar prisms were prepared for each specimen, twelve mortar prisms overall. The related mechanical properties and their coefficients of variation are shown in Table 2.

Hollow clay units are characterized by mean compressive strength

Table 1
Mechanical properties of RC elements.

RC property					
Concrete compressive strength	f_c		42.9	MPa	(CoV = 2.25%)
Steel rebars yielding strength	f_y	ϕ 12	524.5	MPa	(CoV = 1.70%)
		ϕ 10	500.0	MPa	(CoV = 0.87%)
		ϕ 8	503.7	MPa	(CoV = 0.64%)
Steel rebars ultimate strength	f_t	ϕ 12	617.1	MPa	(CoV = 1.33%)
		ϕ 10	596.5	MPa	(CoV = 0.18%)
		ϕ 8	599.0	MPa	(CoV = 0.47%)

Table 2
Mechanical properties of masonry infills.

Masonry property				
Mortar compressive strength	f_{mor}	9.44	MPa	(CoV = 11.3%)
Clay unit compressive strength parallel to holes	f_{bh}	5.00	MPa	(*)
Clay unit compressive strength perpendicular to holes	f_{bv}	2.00	MPa	(*)
Compressive strength parallel to holes	f_{mh}	4.63	MPa	(CoV = 14.4%)
Compressive strength perpendicular to holes	f_{mv}	2.37	MPa	(CoV = 15.3%)
Elastic modulus parallel to holes	E_{mh}	3452	MPa	(CoV = 17.1%)
Elastic modulus perpendicular to holes	E_{mv}	1891	MPa	(CoV = 18.0%)
Tensile strength	f_{mt}	0.29	MPa	(CoV = 14.5%)
Shear modulus	G_m	1622	MPa	(CoV = 15.0%)

(*) Lower bound value provided by the producer.

values perpendicular and parallel to holes (f_{bv} and f_{bh}, respectively) shown in Table 2. Mean masonry compressive strength (f_m) has been evaluated by means of three 750 × 750 × 80 mm^3 masonry wallets tested perpendicularly (f_{mv}) and three equal specimens tested parallel (f_{mh}) to the holes according to the European standard [35]. Corresponding Young modulus have been evaluated by means of the same tests, and the related mean values are reported in Table 2. Mean masonry tensile strength (f_{mt}) and shear modulus (G_m) (see Table 2) were also evaluated on three 1250 × 1250 × 80 mm^3 wallets, by means of diagonal compression tests carried out according to the American standard [36]. For each property, the CoV is also reported in Table 2.

2.3. Loading protocol, setup and instrumentation

The first specimen was tested under out-of-plane loading only. The remaining three specimens were first damaged under in-plane actions and, then, tested under out-of-plane loading. Therefore, the experimental setup is made up of two main parts: the first one is related to the application of the in-plane action (Fig. 2a); the second one is needed for the application of the out-of-plane load (Fig. 2b).

About the IP action, the specimen was first rigidly fixed to the strong floor of the laboratory by means of two steel stiff beams with pre-stressed rods and horizontal steel constrains. Two stiff steel plates were located at the top beam ends and were connected to each other by means of pre-stressed rods. No axial load was applied on columns (as in

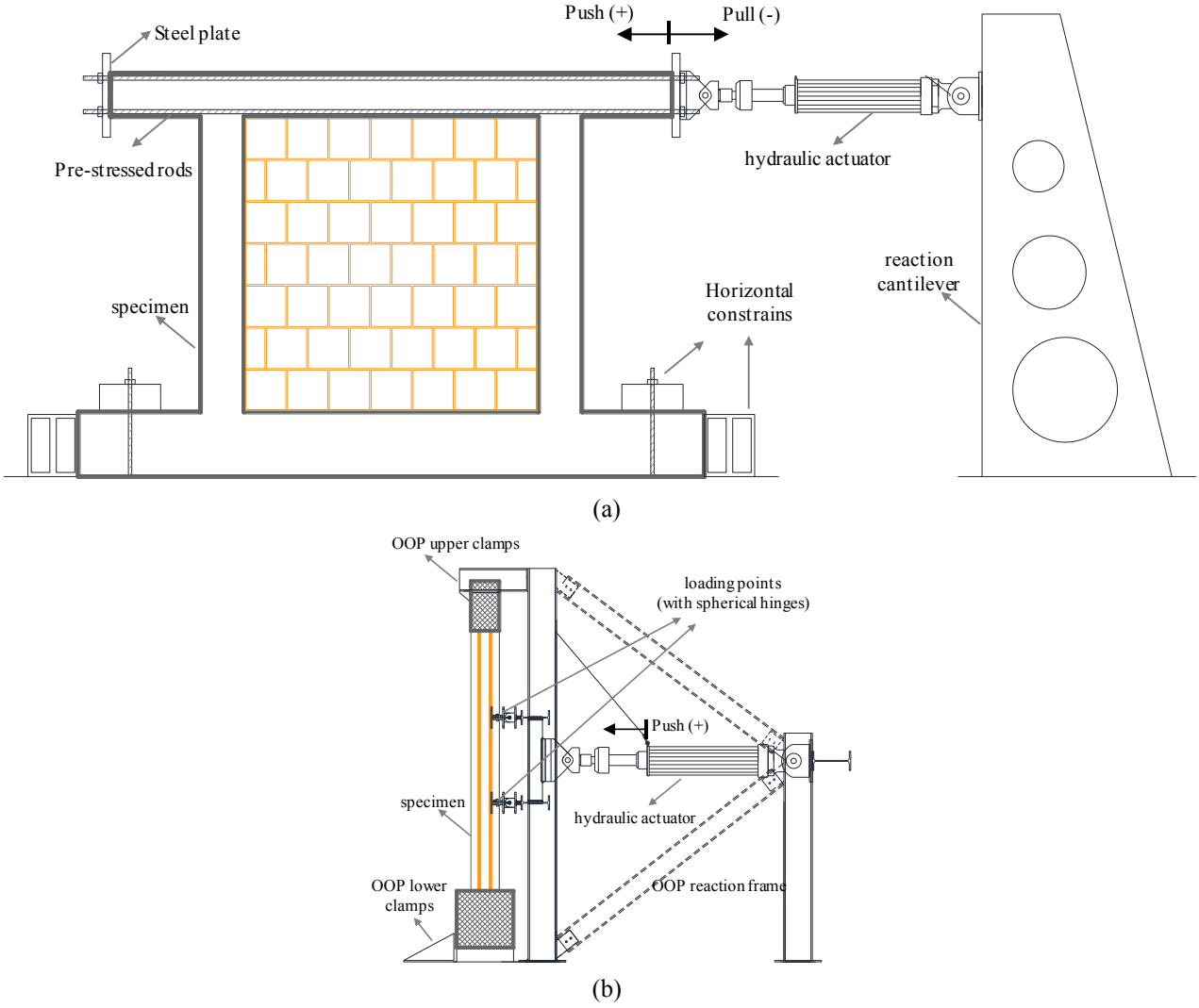

Fig. 2. Experimental setup for in-plane (a) and out-of-plane (b) tests.

Table 3
Imposed nominal in-plane displacement history.

Cycle #	IP drift (%)	IP displacement (mm)	N. of cycles per drift (–)	IP level #
1	0.1	1.97	3	
2	0.2	3.93	3	IP_L (Low)
3	0.3	5.90	3	
4	0.4	7.86	3	IP_M (Medium)
5	0.5	9.83	3	
6	0.6	11.79	3	IP_H (High)

the companion experimental campaign by Ricci et al. [24]. Then a hydraulic actuator – externally constrained to a rigid cantilever – applied a cyclic displacement history at one top beam end, according to the pattern shown in Table 3, up to the "IP levels" IP_L, IP_M, or IP_H, depending on the test, as better described in Section 3. Note that the IP drift values reported in Table 3 are calculated as the ratios between IP displacements and beam centreline distance from the top face of the foundation beam. Note also that, even if higher values of in-plane drift can be reached in design or analysis of infilled RC frames, these drift levels are equal to those already adopted in the previously performed experimental campaign [24] related to rectangular infills, for a sake of comparison. In addition, these drift levels fall down within the typical range of drift capacity values of thin hollow clay infills from Slight Damage State (DS1) to Severe Damage State (DS3), as reported in De Risi et al. [37] and Del Gaudio et al. [38].

About the OOP setup, an external steel frame was adopted as a reaction frame for the hydraulic actuator that applied the OOP displacements. Steel clamps were also used at the top of the beam to restrain potential OOP displacements of the RC frame during the OOP-testing procedure. OOP increasing displacements were monotonically applied with 0.02 mm/s increments. OOP load was applied by means of four points/spherical hinges. The loading points were placed on the infill's diagonals, at a distance from both diagonal's ends equal to one-third of the diagonal length (as in [7,15,24,25]), as shown in Fig. 2b and in Fig. 3. Additional details about the adopted setup can be found in Ricci et al. [24].

Fig. 3 shows the instrumentation layout used during the tests to monitor the IP and OOP responses. About the IP loading, two Linear Variable Displacement Transducers (LVDTs) were located (in IP direction) at the beams' centrelines to monitor the applied IP drift, and constrained to external fixed points. Twelve horizontal LVDTs were located (in OOP direction) all around the infill-concrete edges to monitor eventual detachments. Five laser transducers – fixed to external points – measured the OOP displacement at the centre of the panel and at the points corresponding to the OOP load application. Two LVDTs measured the OOP displacement of the top and bottom beams (at their centreline) to deprive the total OOP applied displacement of eventual displacements of the surrounding RC frame. An additional LVDT was

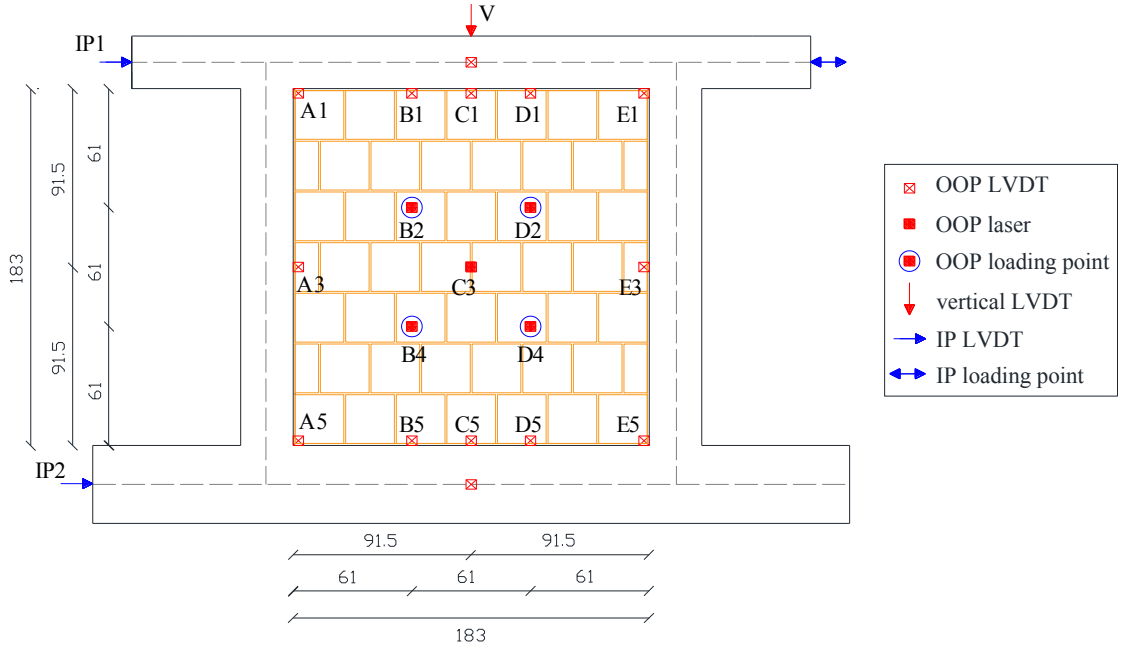

Fig. 3. Instrumentation layout.

finally located in the vertical direction on the top face of the upper beam; its measures will be discussed in detail in the next section.

3. Experimental tests' results

In this section, the results of the experimental tests are shown and commented. First, the response of the purely OOP test, used as a reference, is described in Section 3.1. Then, the combined IP/OOP tests for increasing IP damage level (from IP_L to IP_H, as introduced in Table 3) are analysed in Sections 3.2–3.4. For each test, the OOP force-displacement response is shown, together with the OOP displacements of the control points of the infill panel, the vertical displacement measures of the top beam, and the evolution of the damage pattern. For the combined IP/OOP tests, also the cyclic IP base shear-drift responses are reported and commented.

Each IP test ended at the attainment of the maximum nominal IP drift target (see Table 4); whereas OOP tests were interrupted when the test specimen presented an extensive damage level preventing a further OOP pushing. Note that the maximum actual drifts achieved during the IP tests were always lower than the maximum nominal drifts imposed by the hydraulic actuator because of some "parasitic" displacements, mainly due to the reaction cantilever deformability. Anyway, actual applied displacements will be considered in the following analyses. The comparison between nominal and actual drift levels is shown in Table 4.

3.1. Pure OOP test

The first experimental test has been performed under OOP loading only. Fig. 4 reports the experimental response in terms of OOP force (hereinafter F_{OOP}) versus OOP displacement of the central point of the infill panel (hereinafter referred to as d_{OOP}). The main characteristic points of this response are highlighted in Fig. 4 and reported in Table 5, where K_{sec} represents the ratio between force and corresponding displacement in the ascending part of the response. The secant stiffness at the end of the test has been calculated by means of a linear interpolation of the softening branch of the F_{OOP}-d_{OOP} response from the peak point to the last point of the response, imposing that the starting point of the related softening line coincides with the peak point of the response. Therefore, K_{sec} at the end of the test assumes a negative value.

After an initial elastic branch of behaviour up to F_{OOP} equal to about 7.5 kN, the initial stiffness slightly reduces up to a first visible cracking of the infill, at F_{OOP} = 20.12 kN and d_{OOP} equal to about 2 mm

Table 4
Main characteristics of the experimental tests presented herein.

Test ID	Test typology	Max nominal IP drift (%)	Max actual IP drift (%)
OOP	OOP loading only	0.00	0.00
IP_L-OOP	IP/OOP loading	0.20	0.15
IP_M-OOP	IP/OOP loading	0.40	0.28
IP_H-OOP	IP/OOP loading	0.60	0.51

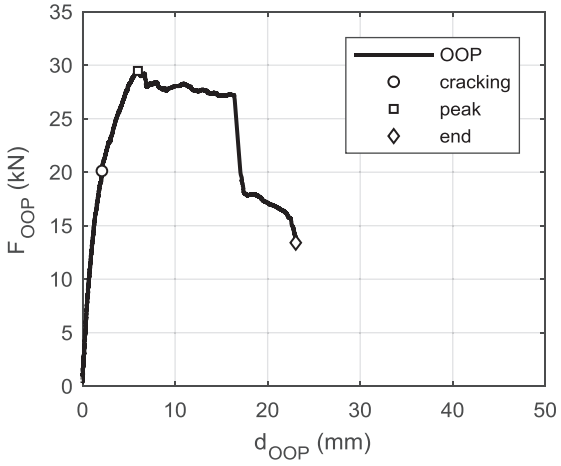

Fig. 4. OOP force-displacement response of OOP test.

Table 5
"OOP" test: OOP force-displacement characteristic points.

"OOP"	Cracking	Peak	End
F_{OOP} (kN)	20.12	29.46	13.41
d_{OOP} (mm)	2.09	5.98	23.04
K_{sec} (kN/mm)	9.62	4.93	−0.71

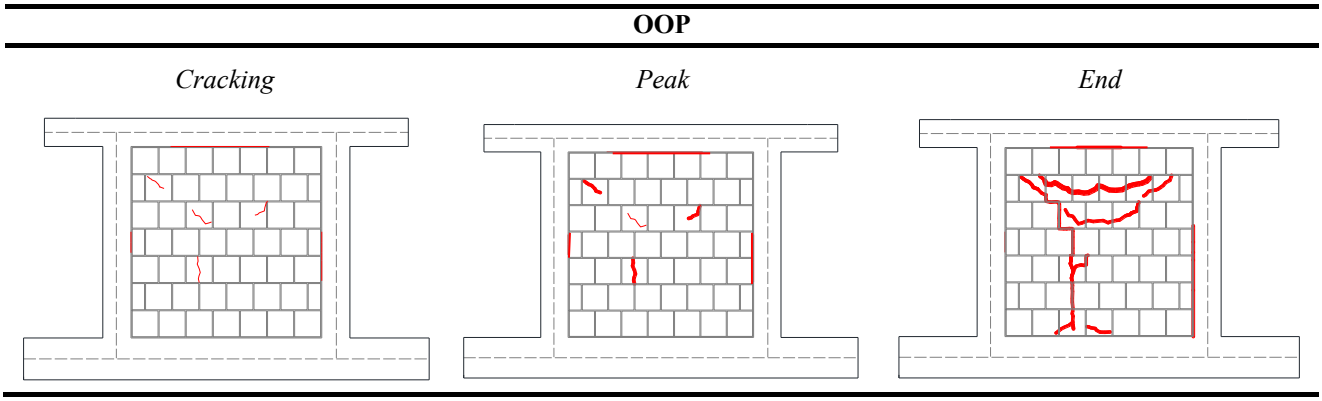

Fig. 5. Damage condition evolution for "OOP" test.

(Table 5). After this macro-cracking, the stiffness further decreases up to the achievement of the OOP peak load, equal to 29.46 kN, at d_{OOP} roughly equal to 6 mm (see Table 5). From macro-cracking to peak strength, existing cracks become wider particularly in the centre of the panel, as shown in Fig. 5. The damage conditions reported in Fig. 5 represent the condition of damage observed in three particular steps of each test: (i) the first cracking in the panel, (ii) the achievement of the peak load, (iii) the end of the test. Wider cracks are marked with thicker lines. During the test, slight local damage of some tiles of the clay units occurs at the infill-frame interfaces, as highlighted by the lines along the edges in Fig. 5. No significant relative displacements between the infill panel and the surrounding beam/columns were observed.

The peak point is followed by a very slight strength drop and an almost constant strength branch until d_{OOP} equal to 16.4 mm is reached, characterised by the extension of the existing cracks throughout the central portion of the infill panel. At d_{OOP} = 16.4 mm a significant drop of F_{OOP} occurs (reaching F_{OOP} = 17.5 kN), mainly due to the failure of the vertical strength arching mechanism, as proved by the experimental displacements provided by the vertical LVDT on the top face of the upper beam (d_V) shown in Fig. 6. Actually, d_V progressively increases as the vertical compressive arch strength mechanism develops within the infill panel until the attainment of its failure due to the attainment of the compressive masonry strength (at d_{OOP} = 16.4 mm d_{OOP}). After this point, the vertical compressed arch suddenly unloads, and d_V rapidly decreases, together with F_{OOP}, until the end of the test. The test ended at F_{OOP} equal to 13.41 kN and d_{OOP} = 23.04 mm (Table 5), corresponding to a strength reduction equal to 54% with respect to the peak point.

The evolution of the OOP deformed shape of the infill panel from macro-cracking to the end of the test (shown in Fig. 7) is obtained from displacement measures provided by LVDTs along the infill edges and laser transducers located on the panel. The deformed shape of the infill panel appeared quite symmetric until the end of the test. Two pictures of the finale damage state are shown in Fig. 8.

3.2. Test IP_L – OOP

In this section, the IP_L-OOP combined IP/OOP test is analysed. First, the IP displacement history shown in Table 3 is applied until the IP_L level, corresponding to a maximum IP nominal drift equal to 0.2% (IP displacement, d_{IP}, equal to 3.93 mm). As mentioned before, due to the in-plane setup deformability, an actual in-plane maximum drift equal to 0.15% (namely, 2.95 mm) is achieved during the test. The cyclic IP response (see Fig. 9a) appears quite symmetric. First visible cracks occurred at F_{IP} equal to +86.9/−88.0 kN at +1.9/−2.1 mm of d_{IP}, involving some clay units and mortar courses in the central part of the panel (see Fig. 10). The IP test has been interrupted at a nominal drift of 0.2%, at F_{IP} equal to −92.0/+99.1 kN, right after the first IP macro-cracking. Therefore, the damage state at the end of the IP test is very similar to damage state at first IP cracking, as shown in Fig. 10. No softening branch of the IP response can be observed, so that it can be argued that the IP peak load of the infilled frame was not yet reached for this test.

After the IP test, the specimen is unloaded to begin the OOP testing procedure. Fig. 9b reports the experimental response in terms of F_{OOP} versus d_{OOP}, together with its main characteristic points (cracking, peak load, end of the test). The corresponding coordinates and damage states are also shown in Table 6 and Fig. 10, respectively. Displacement measures of $LVDT_V$ during the OOP test are shown in Fig. 11.

A first visible cracking on the infill panel is observed at F_{OOP} = 16.15 kN and d_{OOP} equal to 3.50 mm (Table 6). After macro-cracking, the stiffness gradually decreases up to the achievement of the OOP strength, equal to 31.45 kN, at d_{OOP} = 10.43 mm (see Table 6). From macro-cracking to peak strength, existing cracks become wider and spreads particularly in the centre of the panel, as shown in Fig. 10. Also during this test, slight local damage of some tiles of the clay units

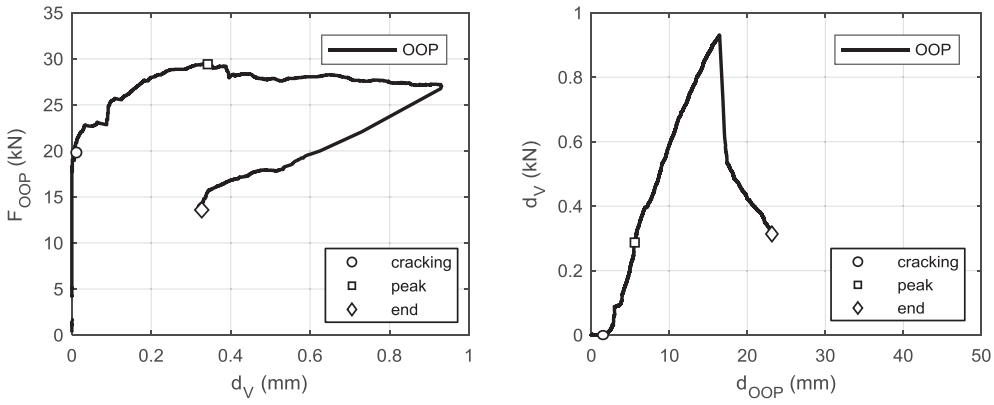

Fig. 6. Vertical displacement of the top face of the upper beam for "OOP" test.

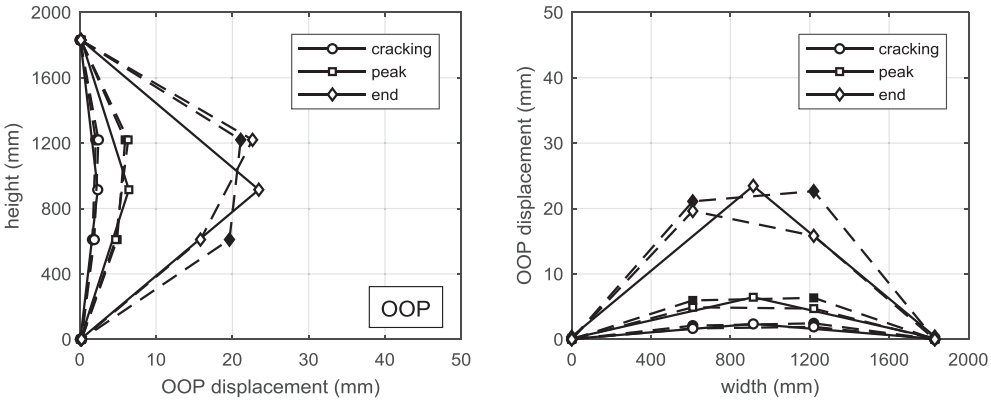

Fig. 7. Evolution of the OOP displacement of the infill panel for test "OOP".

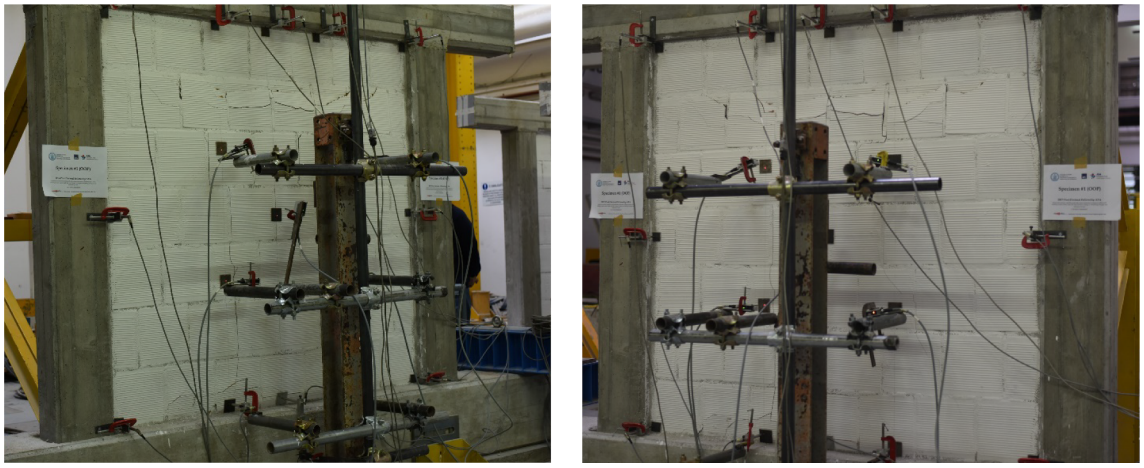

Fig. 8. End of "OOP" test.

occurs at the infill-frame interface, as shown in Fig. 10. No significant relative displacements between the infill panel and the surrounding beam/columns were observed.

The peak point is followed by a significant strength drop (reaching F_{OOP} = 21.8 kN), characterised by the extension of the existing cracks throughout the central portion of the infill panel. Also in this case, the significant OOP strength drop corresponds to the failure of the vertical strength arching mechanism, as proved by the d_V evolution shown in Fig. 11. The strength drop is followed by an almost constant load branch up to about 15.5 mm, while the vertical compressed arch is unloading. After this point, d_V rapidly decreases together with F_{OOP}, until the end of the test.

OOP test was stopped at F_{OOP} equal to 12.69 kN and d_{OOP} = 20.78 mm (Table 6), corresponding to a strength reduction equal to 60% with respect to the peak point. The final state of the specimen is shown in Fig. 12.

3.3. Test IP_M – OOP

IP_M-OOP combined test is analysed here. For this test, the IP displacement history shown in Table 3 is applied until the IP_M level, corresponding to a maximum IP nominal drift equal to 0.4% (IP displacement, d_{IP}, equal to 7.86 mm). Due to the in-plane setup

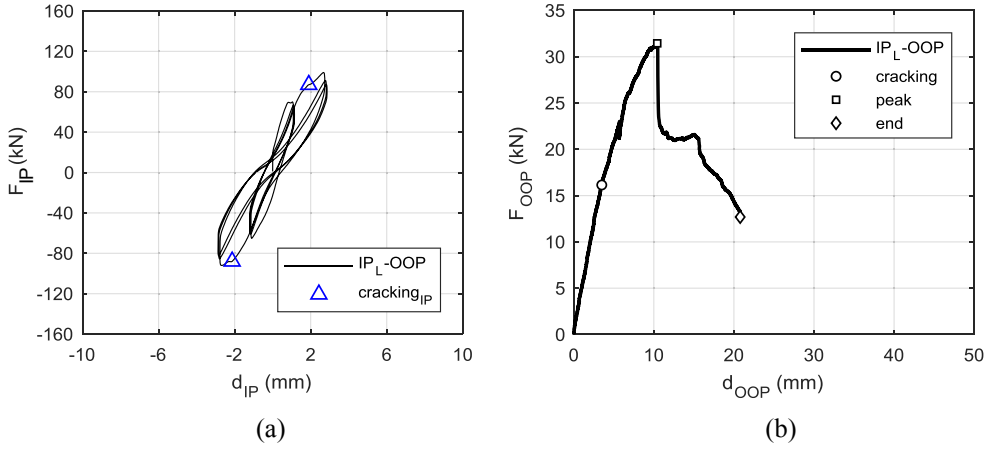

Fig. 9. IP (a) and OOP (b) force-displacement response of IP_L-OOP test.

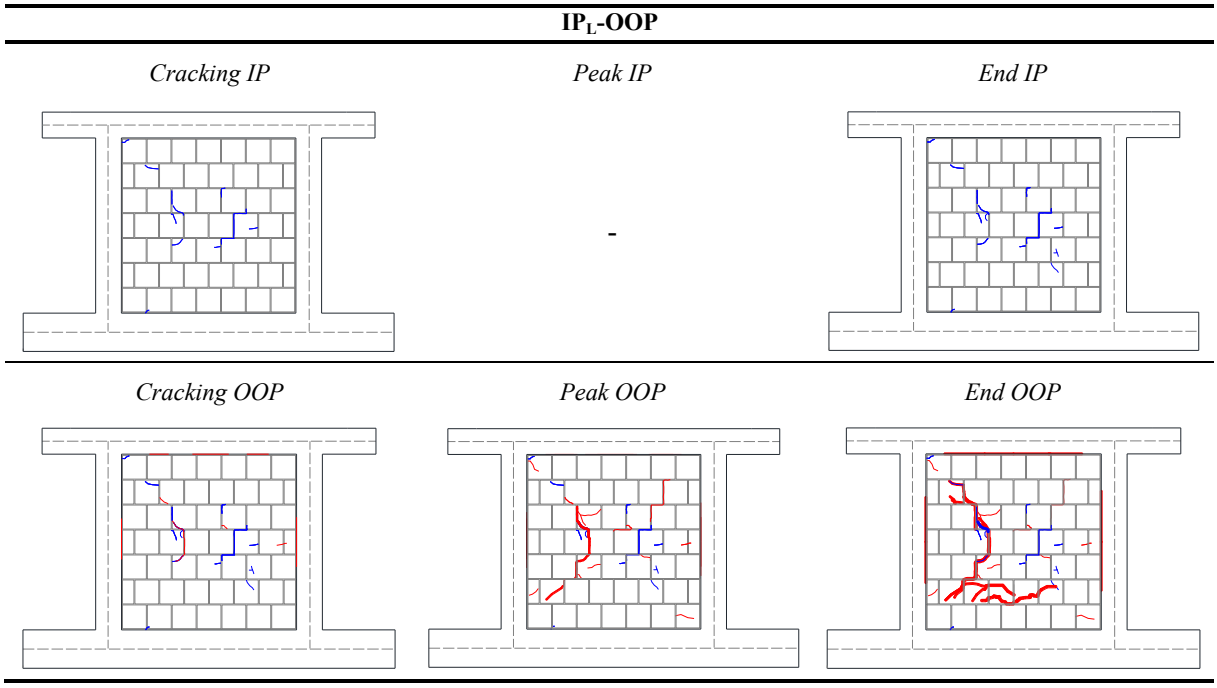

Fig. 10. Damage condition evolution for IP$_L$-OOP test (blue lines represent cracks appeared during the IP test, red lines during the OOP test).

Table 6
IP$_L$-OOP test: OOP force-displacement characteristic points.

IP$_L$ – OOP	Cracking	Peak	End
F_{OOP} (kN)	16.15	31.45	12.69
d_{OOP} (mm)	3.50	10.43	20.78
K_{sec} (kN/mm)	4.61	3.02	−2.04

deformability, the actual in-plane maximum drift achieved during the test is equal to 0.28% (namely, 5.50 mm). The resulting cyclic IP response is shown in Fig. 13a. It appears quite asymmetric in terms of F_{IP}, likely due to an asymmetric damage evolution during the imposed displacement cycles. First visible cracks occurred at F_{IP} equal to +104.62/−55.34 kN at +2.5/−1.2 mm of d_{IP}, mainly involving central mortar courses and only few clay units (see Fig. 14). The IP test has been interrupted at a nominal drift of 0.4%, at F_{IP} equal to −104.0/+142.6 kN. The final damage state shows the spreading of existing cracks and the onset of new hairline cracks (Fig. 14). No softening branch of the IP response can be observed; therefore, also in this case the IP peak load of the infilled frame was not yet reached.

At the end of the IP test, the specimen is unloaded to begin the OOP testing procedure. Fig. 13b reports the experimental response in terms of F_{OOP} versus d_{OOP}, and its main characteristic points. The corresponding coordinates and damage states are also shown in Table 7 and Fig. 14, respectively.

A first visible cracking on the infill panel is observed at F_{OOP} = 15.21 kN and d_{OOP} equal to 5.16 mm (Table 7). After the first macro-cracking existing cracks become wider and spread particularly in the centre of the panel; new cracks also appeared in the central portion of the infill, as shown in Fig. 14. Slight local damage of some tiles of the clay units occurs at the infill-frame interface (see red lines along the interfaces in Fig. 14).

The tangent stiffness gradually reduces, becoming equal to zero at F_{OOP} equal to about 22 kN, where an almost constant branch starts (from d_{OOP} equal to 8.3 mm to about 15.5 mm). OOP strength (equal to 22.49 kN) is achieved at d_{OOP} = 12.86 mm (see Table 7). The peak point is followed by a strength drop (up to F_{OOP} = 16.8 kN), characterised by the extension of the existing cracks throughout the panel, including its upper and lower portions. The strength drop corresponds to a significant d_V reduction (which was increasing up to the peak load), proving the failure of the vertical strength arching mechanism (see Fig. 15). The strength drop is followed by a quite soft degrading up to

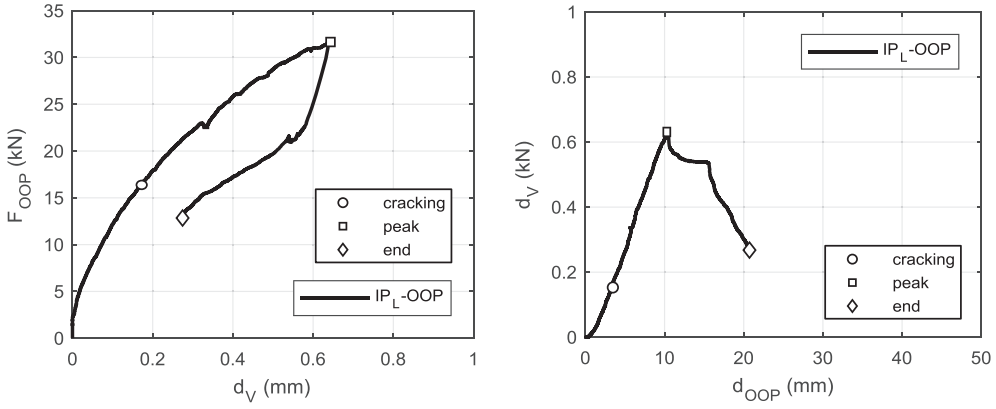

Fig. 11. Vertical displacement of the top face of the upper beam for IP$_L$-OOP test.

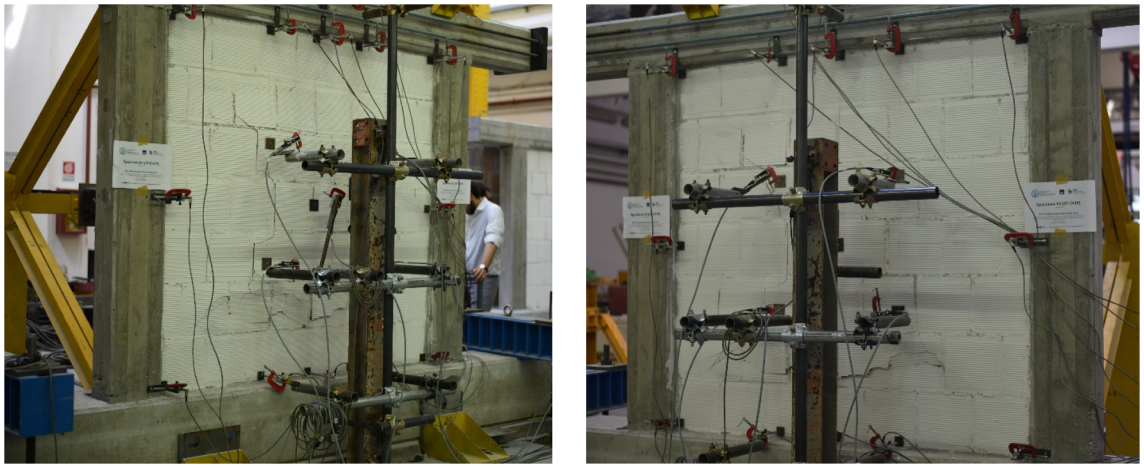

Fig. 12. End of IP_L-OOP test.

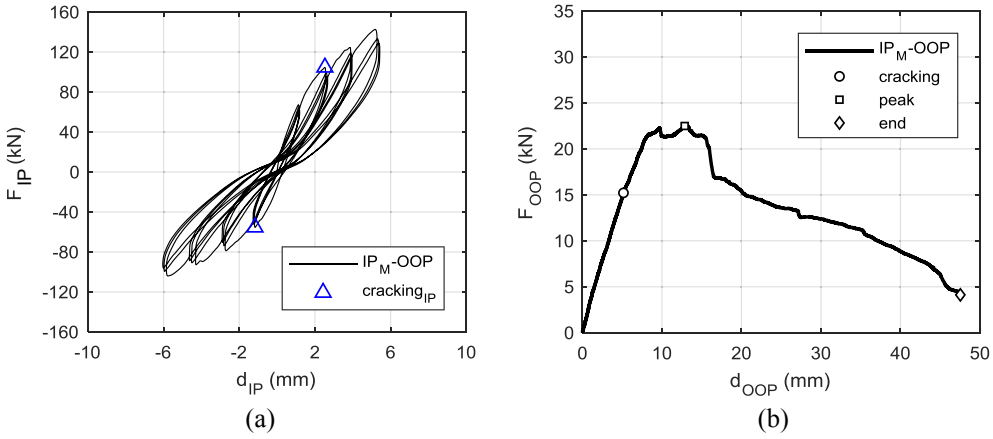

Fig. 13. IP (a) and OOP (b) force-displacement response of IP_M-OOP test.

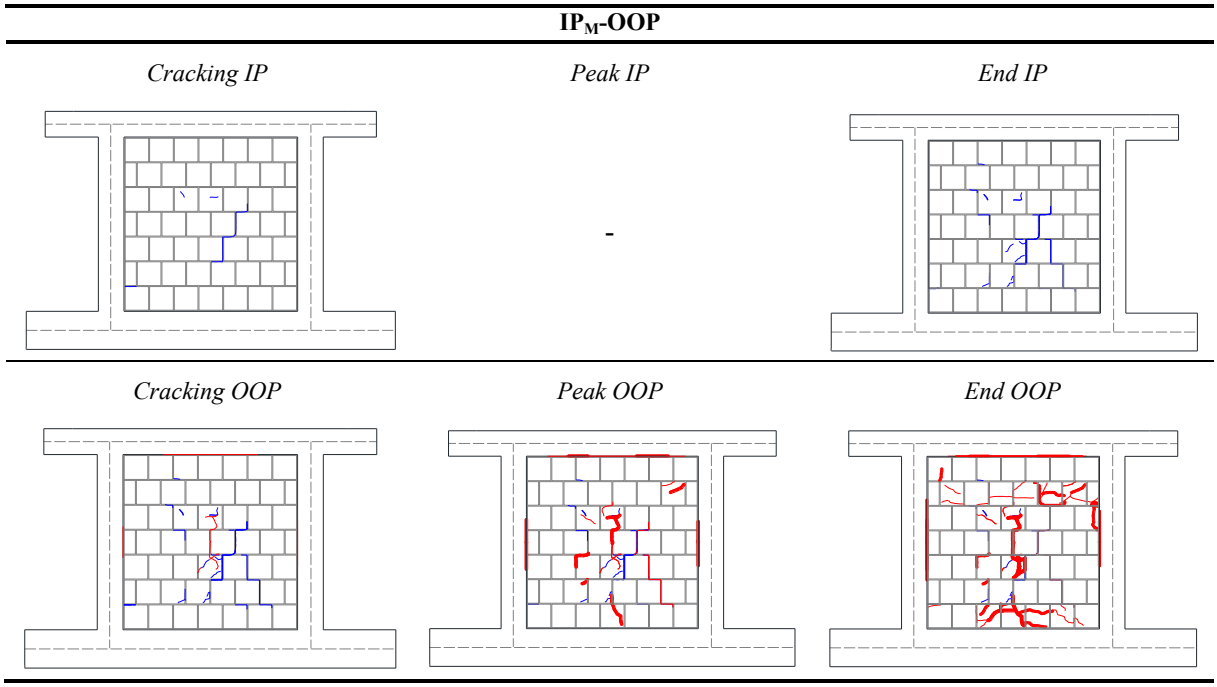

Fig. 14. Damage condition evolution for IP_M-OOP test (blue lines represent cracks appeared during the IP test, red lines during the OOP test).

Table 7
IP_M-OOP test: OOP force-displacement characteristic points.

IP_M – OOP	Cracking	Peak	End
F_{OOP} (kN)	15.21	22.49	4.12
d_{OOP} (mm)	5.16	12.86	47.53
K_{sec} (kN/mm)	2.95	1.75	−0.55

the end of the test, at d_{OOP} = 47.53 mm and F_{OOP} = 4.12 kN (see Table 7), corresponding to a strength reduction equal to 82% with respect to the peak point. The final state of the specimen is shown in Fig. 16.

3.4. Test IP_H – OOP

The maximum IP nominal drift applied for this test is equal to 0.6% (IP displacement, d_{IP}, equal to 11.79 mm). Due to the in-plane setup deformability, the actual in-plane maximum drift achieved during the test is equal to 0.51% (namely, 10.02 mm). The resulting IP cyclic response is quite symmetric, as shown in Fig. 17a. A bi-linear response can be clearly identified, with a first branch from the origin to the first macro-cracking, and a second branch from the cracking point up to the maximum achieved F_{IP} (at the last imposed displacement cycle). No softening phase can be observed. The first visible cracks in some clay units (see Fig. 18) occurred at F_{OOP} = +88.80/−94.19 and d_{OOP} = +2.02/−2.40 mm. For increasing IP applied displacements, first cracks become wider and new cracks developed throughout the panel, together with some quite significant detachments between the infill panel and the upper beam and the columns (Fig. 18). The IP test has been interrupted at a nominal drift equal to 0.6%, at F_{IP} equal to −148.4/+151.9 kN.

Then, the OOP testing procedure was applied, as for previous tests. The resulting OOP response is shown in Fig. 17b, where also first OOP macro-cracking, peak load and end of the test have been highlighted.

A first visible cracking on the infill panel and slight detachments between infill and RC columns are observed at F_{OOP} = 11.61 kN and d_{OOP} equal to 7.49 mm (Table 8). After the first macro-cracking existing cracks become wider and spread particularly in the centre of the panel; new cracks also appeared in the central and in the top portions of the infill, as shown in Fig. 18. Local damage of some tiles of the clay units occurs at the infill-frame interfaces also for this test, more significant due to the higher applied IP drift with respect to the previous tests.

The tangent stiffness gradually reduces up to OOP strength (equal to 19.21 kN) is achieved, at d_{OOP} = 18.02 mm (see Table 8). The peak point is followed by a strength drop (up to F_{OOP} = 15.5 kN), characterised by the extension of the existing cracks throughout the panel (Fig. 18). The strength drop corresponds to the beginning of the d_V reduction, which was increasing up to the peak load (see Fig. 19). The strength drop is followed by a quite soft degrading branch up to the end of the test, at d_{OOP} = 48.99 mm and F_{OOP} = 5.08 kN (see Table 8), corresponding to a strength reduction equal to 74% with respect to the peak load. The final damage state of the specimen is shown in Fig. 20.

3.5. Comparison and discussion

The experimental tests described in detail in the previous sections are compared each other in this section, both in terms of IP and OOP response (see Fig. 21).

About the IP tests, Fig. 21a shows the envelopes of the responses of the three tests performed with different maximum nominal IP drift. They appear very similar each other, especially in the initial phase and in the positive direction (the first pushing direction). Actually, this outcome was expected due to the nominally identical mechanical and geometrical properties of all the specimens. Also first macro-cracking due to IP actions appeared at very similar imposed drift levels. Maximum achieved in-plane base shear F_{IP} increases with the applied drift from IP_L-OOP to IP_H-OOP; no degrading branches can be observed in any in-plane test, as already highlighted in the previous sections.

Additionally, for the IP tests, a relationship between the observed damage (see Figs. 10, 14, and 18) and Damage States (DSs) definitions existing in the literature can be found. In particular, DSs definitions proposed by Cardone and Perrone [39] are adopted herein, as recently suggested in Del Gaudio et al. [38]. Based on these definitions, it can be stated that DS1 (*Slight Damage State*) has been attained in tests IP_L and IP_M, at the end of the tests, due to the occurrence of slight diagonal small cracks in the center of the panels. In test IP_H, DS2 (*Moderate Damage State*) can be considered reached at the end of the test, due to the extension of previously born diagonal cracks and the localization of damage units and wider cracks close to the top corners of the panel.

Fig. 21b shows the comparison of the OOP responses. First, it can be noted that the “reference” test “OOP” (in black) is characterized by the stiffest initial branch of the F_{OOP}-d_{OOP} response, as expected due to the absence of any IP damage for this test. Due to the increasing IP damage from IP_L-OOP to IP_H-OOP test, this stiffness progressively reduces; in tune, K_{sec} both at first-cracking and at peak load decreases when the IP damage increases, as confirmed by data shown in Table 5, Table 6, Table 7, and Table 8. The OOP displacement corresponding to the peak load progressively increases with increasing IP damage; whereas, maximum F_{OOP} generally decreases with increasing IP damage level, as expected. The only exception to this trend is the IP_L-OOP test, for which maximum F_{OOP} results slightly (about 7%) higher than maximum F_{OOP} related to the “reference” IP-undamaged test. Given the very low IP drift level and IP damage reached during this test, such an evidence can be only attributed to an unavoidable experimental variability, generally very pronounced for infill masonry walls, rather than to some questionable mechanical bases.

Finally, note that the post-peak behaviour of the OOP responses

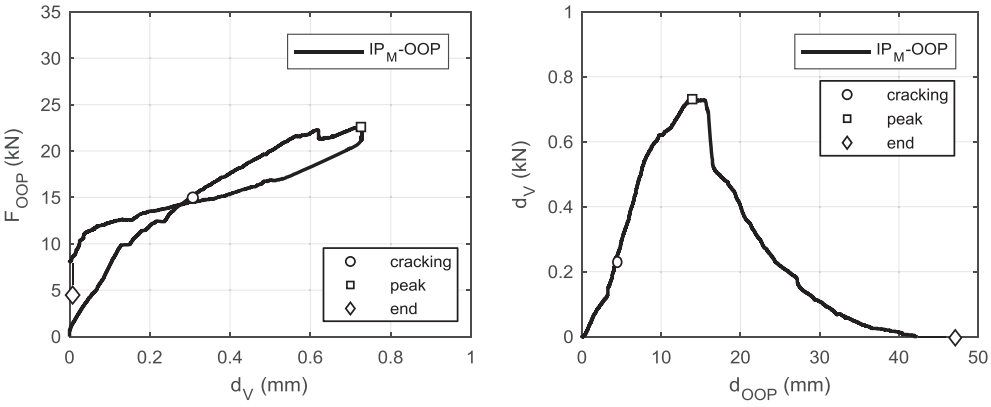

Fig. 15. Vertical displacement of the top face of the upper beam for IP_M-OOP test.

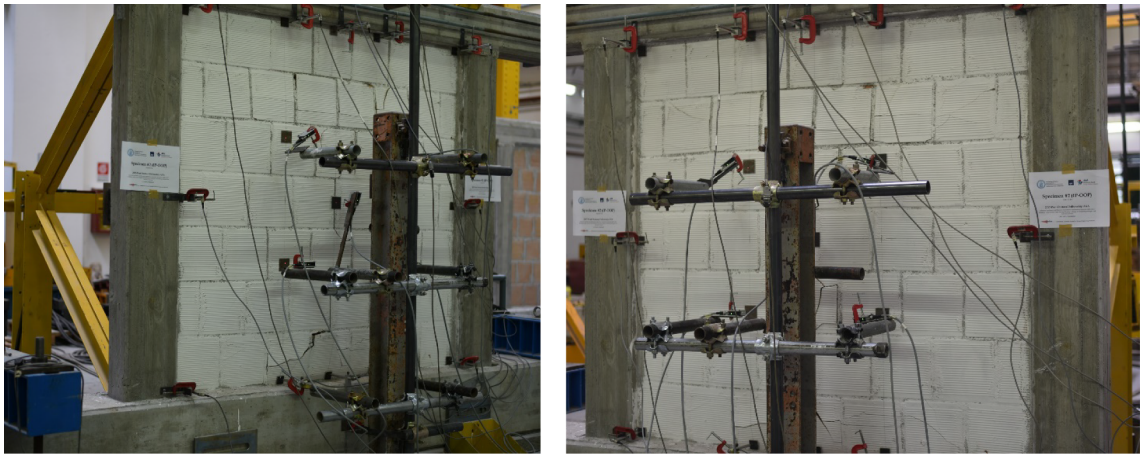

Fig. 16. End of IP_M-OOP test.

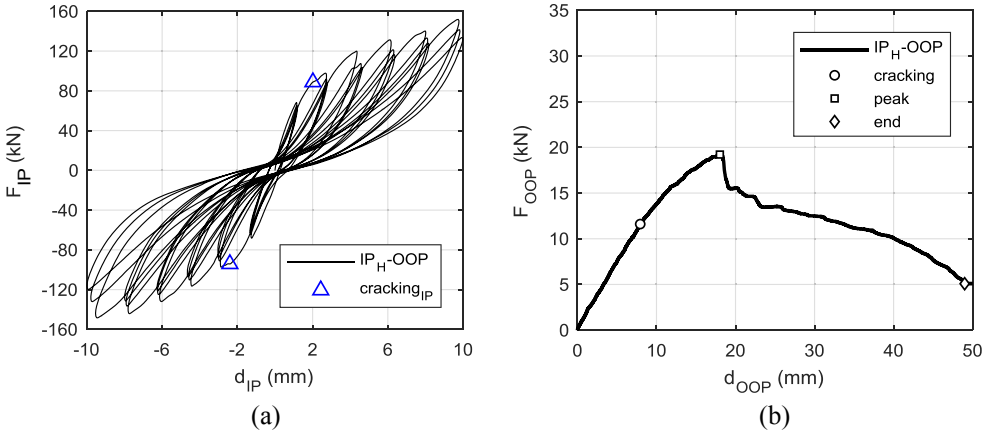

Fig. 17. IP (a) and OOP (b) force-displacement response of IP_H-OOP test.

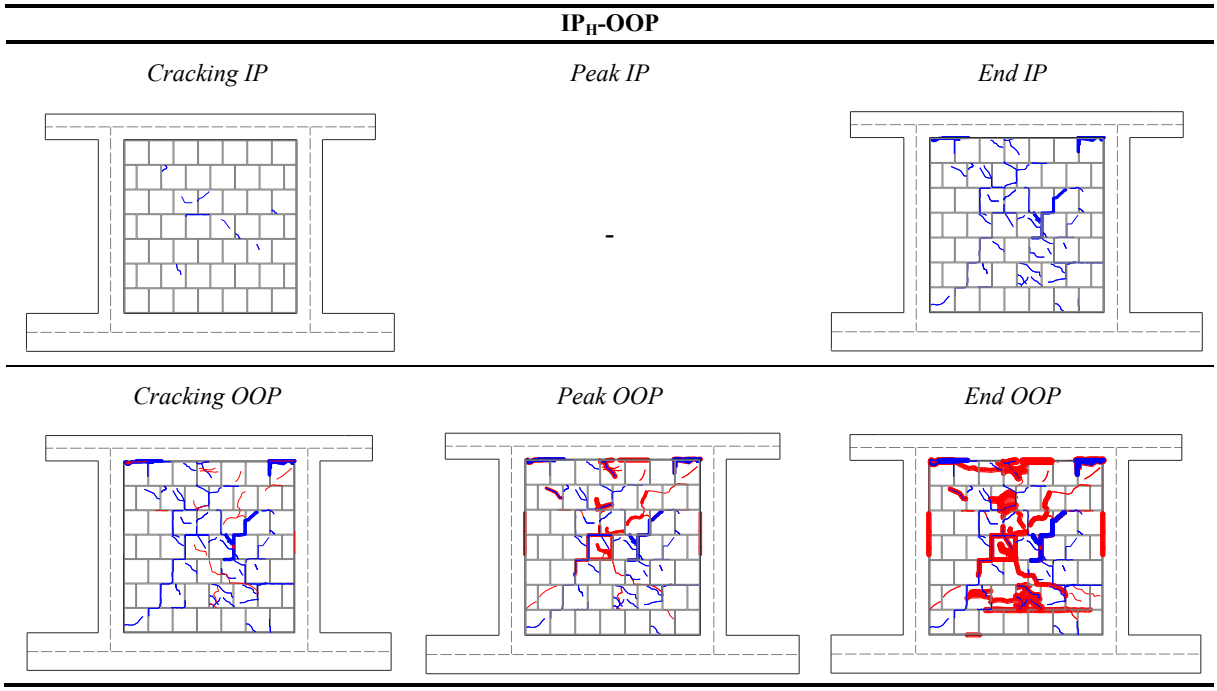

Fig. 18. Damage condition evolution for IP_H-OOP test (blue lines represent cracks appeared during the IP test, red lines during the OOP test).

Table 8
IP_H-OOP test: OOP force-displacement characteristic points.

IP_H – OOP	Cracking	Peak	End
F_{OOP} (kN)	11.61	19.21	5.08
d_{OOP} (mm)	7.94	18.02	48.99
K_{sec} (kN/mm)	1.46	1.07	−0.48

seems to follow a common, quite soft, degrading branch, especially after the peak load and the subsequent strength drop were achieved.

4. Assessment of the IP-undamaged specimen OOP strength

In this section, the pure OOP strength of the control specimen (OOP test) is discussed. More specifically, the available literature formulations allowing the assessment of the OOP strength are applied and their results compared with the experimental test results. In addition, Dawe and Seah [1]'s model is applied to obtain a prediction of the complete force-displacement response of the specimen.

As reported in Section 4, the OOP strength of specimen "OOP" was equal to 29.5 kN. The specimen slenderness, both in the vertical and in the horizontal direction, is roughly equal to 23. This value, together with the RC members' cross-sections' inertia, is compatible with the formation of both horizontal and vertical arching resistance mechanism according, e.g., to ASCE SEI 41/13 [40].

In the literature, formulations for the prediction of the OOP strength of URM infills in which two-way arching action occurs are provided by Dawe and Seah [1], Bashandy et al. [4], Flanagan and Bennett [6], Ricci et al. [21].

The formulations by Dawe and Seah [1] and by Flanagan and Bennett [6] are empirical and dedicated to infills under lateral uniformly distributed load. Hence, they are not applicable in the present case.

Bashandy et al. [4]'s formulation is based on mechanical assumptions and has been adapted to the four-point loading condition by Di Domenico et al. [23] as reported in Equation (1).

$$F_{max} = 16M_{yv}\left[\frac{3}{8}\left(2\frac{w}{h} + \frac{M_{yh}}{M_{yv}}\frac{x_{yv}}{x_{yh}} - 1\right)\right] \quad (1)$$

In Eq. (1), M_y is the infill resisting moment associated with vertical (v subscript) and horizontal (h subscript) arching. It is expressed in Nmm/mm and can be calculated as reported in Equation (2).

$$M_y = \frac{1}{8}0.85f_m t^2\left(1 - \frac{f_m}{E_m\varepsilon_c}\right)^2 \quad (2)$$

In Eq. (1), f_m is masonry compressive strength expressed in N/mm^2, t is the infill thickness in mm, E is masonry elastic modulus in N/mm^2, ε_c is masonry limit strain calculated according to Eq. (3).

$$\varepsilon_c = \frac{\sqrt{(L/2)^2 + t^2} - L/2}{\sqrt{(L/2)^2 + t^2}} \quad (3)$$

In Eq. (3), L is the infill length in the considered direction (i.e., the infill height for vertical arching or the infill width for horizontal arching), t is the infill thickness.

In Eq. (1), x_y is the OOP central displacement at the attainment of the maximum possible contribution of vertical (v subscript) and horizontal (h subscript) arching to the infill OOP resistance. It is expressed in mm and can be calculated as reported in Eq. (4).

$$x_y = \frac{tf_m}{E_m\varepsilon_c} \quad (4)$$

The application of Eq. (1) provides a predicted OOP strength equal to 11.7 kN for the in-plane-undamaged specimen "OOP", with a significant underestimation (−60%). It should be noted that Bashandy et al. [4] themselves state that their formulation underestimates the actual OOP strength of URM IP-undamaged infills and that it could be used with better effectiveness for IP-damaged infills.

Ricci et al. [21]'s empirical formulation, reported in Eq. (5), was derived based on an experimental database collecting infills laterally loaded with both uniformly distributed and four-point loads. Hence, it can be applied also in the present case.

$$F_{max} = 1.95f_{mv}^{0.35}\frac{t^{1.59}}{h^{2.96}}A \quad (5)$$

In Eq. (5), f_{mv} is masonry vertical compressive strength expressed in N/mm^2, t and h are the infill thickness and height, respectively, expressed in m, A, which is equal to the infill width w times h, is expressed in mm^2. This formulation provides and OOP strength equal to 26.6 kN, with a slight underestimation (−10%) with respect to the experimental value.

Dawe and Seah [1] defined a mechanical model for the construction of the entire OOP force-displacement response of URM infill walls. Such model is based on the application of the Principle of Virtual Works and allows accounting for the effect of the confining frame elements' deformability on such response. The mechanical nature of the model allows its application for infills under whichever loading condition. Verderame et al. [2] described in detail the steps that must be performed for the model application. Herein, the procedure is applied for the "reference" specimen "OOP".

First, a regularized and somehow idealized deformed shape, i.e., a linear relationship between the OOP central displacement and the OOP displacement of whichever point of the panel, must be set for the infill. Clearly, this deformed shape should be reasonably defined based on the real deformed shape exhibited during the test by specimen "OOP". Remember that, of course, the deformed shape of the infill changes during the test, while the application of Dawe and Seah [1]'s model requires the definition of a unique and non-evolving deformed shape.

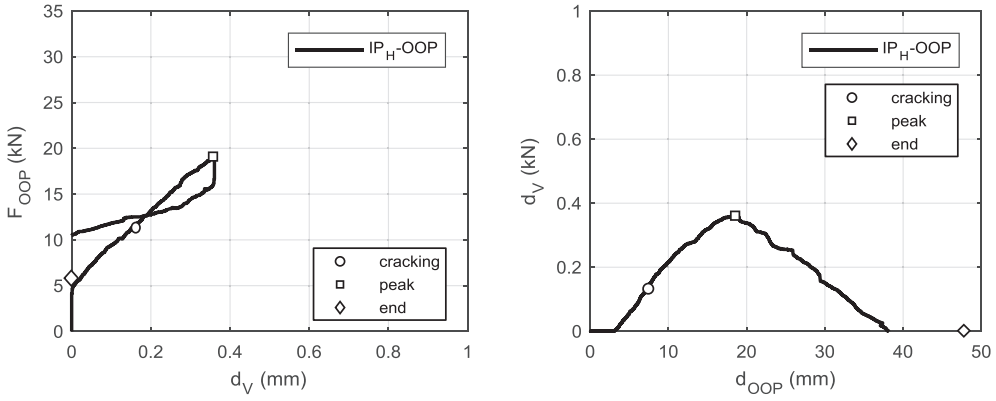

Fig. 19. Vertical displacement of the top face of the upper beam for IP_H-OOP test.

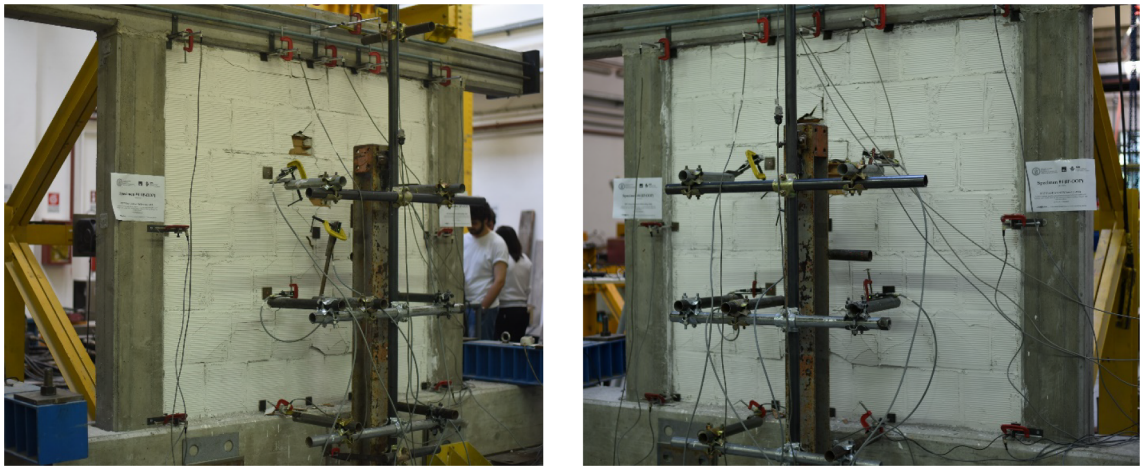

Fig. 20. End of IP_H-OOP test.

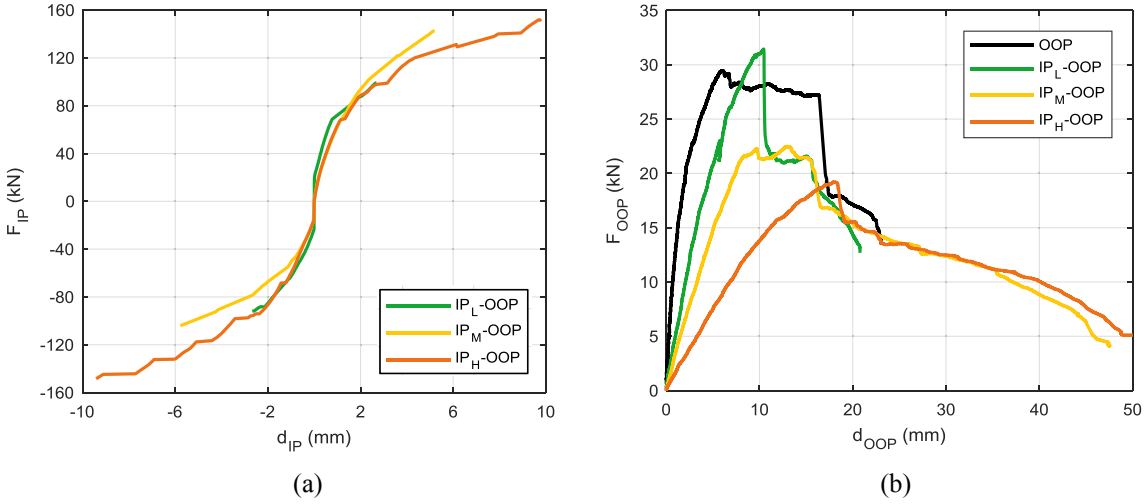

Fig. 21. Comparison among IP (a) and OOP (b) responses of the tested specimens.

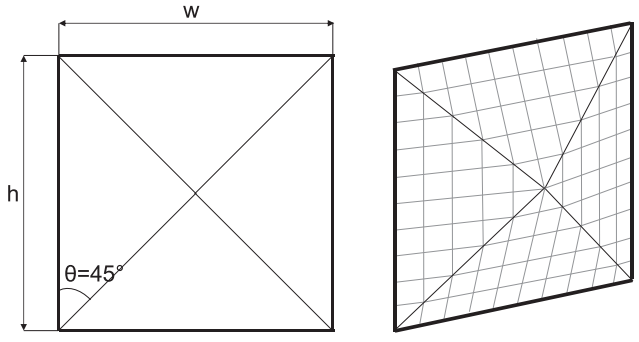

Fig. 22. Idealized deformed shape for specimen "OOP".

The reference deformed shape is herein fixed based on the experimental one exhibited at the attainment of peak load, due to the preeminent importance of such condition in characterizing the response of whichever structural or non-structural element. Note also that, actually, the shape of the curves represented in Fig. 7 is quite independent on the actual entity of the OOP central displacement. The experimental deformed shape of specimen "OOP" at the attainment of peak load along vertical and horizontal alignments have been shown in Fig. 7. Based on these deformed shapes, it seems reasonable to assume that the idealized and regularized deformed shape of the infill can be described, within the application of Dawe and Seah [1]'s model, by a square pyramid, as shown in Fig. 22.

Herein, Dawe and Seah [1]'s model is applied under the hypotheses of:

i. stiff confining RC elements; or
ii. deformable confining RC elements.

To be more specific, point ii. is applied in two ways: first, the RC elements flexural stiffness is calculated based on the gross inertia of the elements' cross section; second, the RC elements flexural stiffness is calculated based on a reduced inertia of the elements' cross section to account for the effects of concrete (and, potentially, steel rebars) non-linearity. The reduction coefficient, equal to 0.35, has been determined in order to obtain a predicted maximum deflection due to arching thrusts of the RC frame upper beam equal to the experimental one, which was read by $LVDT_V$ (see the instruments' layout in Fig. 3) and was roughly equal to 0.9 mm.

In Fig. 23, the experimental OOP force-displacement curve (black line) is compared with the predicted OOP force displacement relationship evaluated under three different assumption (i. – blue continuous line – and ii. with elastic – blue dashed line – and effective – blue dotted line – stiffness of the RC elements). In the same figure, the predicted relationship between the OOP central displacement and the beam deflection is shown in the three cases and compared with the experimental one.

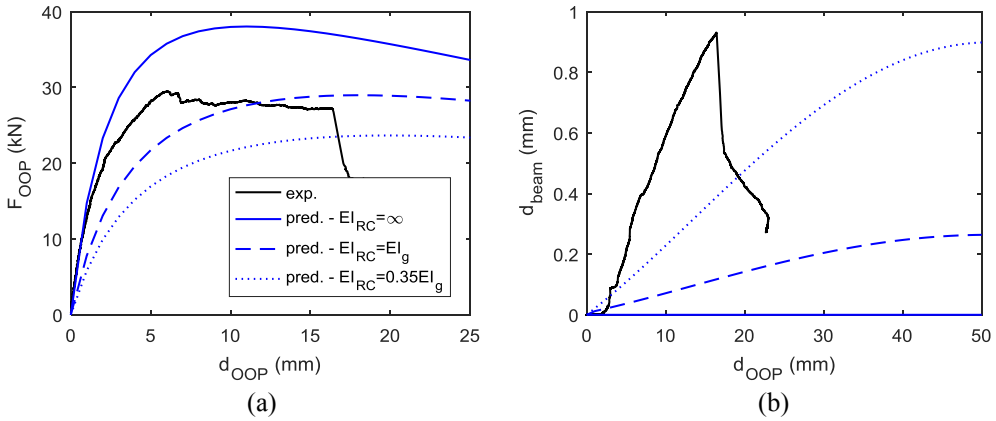

Fig. 23. Experimental and predicted OOP force-displacement relationship (a) and experimental and predicted OOP central displacement-beam deflection relationship (b) for specimen "OOP". The legend reported in the Fig. 23a applies also to Fig. 23b.

It seems from the comparison reported in Fig. 23 that the curve obtained by considering stiff boundary elements is characterized by an initial stiffness in good accordance with the experimental evidence. Namely, the predicted initial stiffness is, in this case, 14.7 kN/mm, while the experimental value is 15.6 kN/mm. However, the hypothesis of stiff confining elements yields to a significant (+29%) overestimation of the specimen strength, with a predicted value equal to 38.0 kN.

To obtain a more realistic prediction, it is necessary to account for the frame elements' deformability. In this case, the stiffness (both the initial and the secant at maximum) of the specimen is underestimated but the strength is very well caught in the case of elastic stiffness of the confining members (with a predicted strength equal to 29.0 kN and an underestimation error equal to less than 2%). However, in this case, the maximum beam outward deflection is highly underestimated, as the predicted value is 0.26 mm.

To obtain a more realistic prediction of the beam outward displacement, an effective stiffness equal to 0.35 times of the elastic one is assigned to RC members. Actually, this value seems to be too small, also considering that the RC frame, in this case, has not been previously damaged by IP actions. In this case, the predicted beam deflection is equal to the experimental one, 0.9 mm, but the specimen stiffness and, above all, strength is significantly underestimated, with a predicted strength equal to 23.7 kN and an underestimation error equal to 20%.

Hence, the OOP strength of the specimen is very well caught by Dawe and Seah [1]'s model if the effect of the deformability of RC members, modelled as elastic, is considered. A summary of the strength predictions obtained by applying the above-discussed models is reported in Table 9.

It is worth to note, as shown in Fig. 24, that the application of the same response model yields to a very good prediction of the experimental response also of the rectangular specimen 80_OOP_4E by Ricci et al. [24], with a very small overestimation of the OOP strength in the case of stiff confining elements (+4%) and with a very small underestimation in the case of deformable confining elements with elastic stiffness (−5%).

5. The influence of the aspect ratio on the IP/OOP interaction effects

One of the main aim of the present research is the assessment of the influence of the aspect ratio of the infill wall, i.e., the width-to-height ratio, on the entity of the IP/OOP interaction effects in terms of strength reduction. To achieve this goal, four proper existing tests from literature have been analysed together with the tests presented in the previous Sections. More in details, four infill walls nominally identical for geometric properties and materials used to those tested for this study, except for the aspect ratio, were subjected to combined IP/OOP tests by Ricci et al. [24]. Four infill walls with the same height (1830 mm) but with width equal to 2350 mm and aspect ratio w/h equal to 1.28 were tested in the OOP direction; three of them had been previously cyclically loaded in the IP direction up to the attainment of the same three nominal drift levels applied in the experimental campaign presented herein (0.20%, 0.40% and 0.60%). During the tests, given the setup slight deformability, the actually attained drifts were equal to 0.16%, 0.37% and 0.58%. The drift set herein investigated and that reported in Ricci et al. [24] still remain comparable, as they are only slightly different.

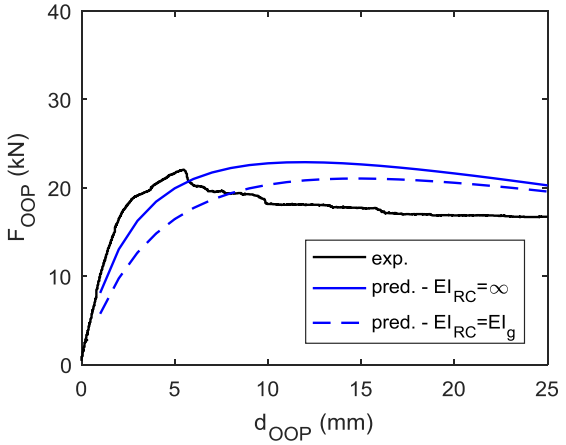

Fig. 24. Experimental and predicted OOP force-displacement relationship for specimen "80_OOP_4E" by Ricci et al. [24].

Therefore, this section is dedicated to two main issues. First, the combined IP/OOP tests' results, together with those obtained on the nominally identical rectangular infills by Ricci et al. [40], are compared with the available formulations proposed in the literature for modelling the IP/OOP interaction effects. Second, the potential deficient

Table 9
Comparison of the experimental (exp) and predicted (pred) values of the OOP strength of specimen "OOP".

	Bashandy et al.	Ricci et al.	Dawe and Seah ($EI_{RC} = \infty$)	Dawe and Seah ($EI_{RC} = EI_g$)	Dawe and Seah ($EI_{RC} = 0.35EI_g$)
Predicted strength	11.7 kN	26.6 kN	38.0 kN	29.0 kN	23.7 kN
exp/pred	2.52	1.11	0.77	1.02	1.24

predictive capacity of such formulations is discussed at the light of the comparison of the results of tests on square and rectangular infills and with reference to the influence of the different aspect ratio on the entity of the IP/OOP interaction effects.

In the literature, different relationships aimed at predicting the IP displacement demand effects on the OOP response of URM infills have been proposed.

The strength reduction factor R (IP damaged-to-IP undamaged strength ratio) can be predicted by using Angel et al. [3]'s formulation, which is reported in Eq. (6). In this case, R depends on the infill slenderness (h/t) and on the IP displacement demand (IDR) normalized with respect to the IP displacement demand at the infill IP first visible cracking (IDR_{crack}).

$$R = \begin{cases} 1 & \frac{IDR}{2IDR_{crack}} < 0.5 \\ [1.08 + (h/t)(-0.015 + (h/t)(-0.00049 + 0.000013(h/t)))]^{\frac{IDR}{2IDR_{crack}}} & \frac{IDR}{2IDR_{crack}} \geq 0.5 \end{cases} \quad (6)$$

The value of the OOP strength degradation factor can be predicted also by the [41] formulation, which is a function only of the value of the infill slenderness (h/t), as reported in Eq. (7).

$$R = \min\left(1.1\left(1 - \frac{h/t}{55}\right); 1\right) \quad (7)$$

The results of the comparison of the experimental data with the predictions by Angel et al. [3]'s and NZSEE formulations are reported in Table 10 and in Fig. 25. Note that the application of Angel et al. [3]'s formulation is performed by assuming as IDR_{crack} for each specimen the average of the positive and negative IDR value at the formation of the first visible crack during IP tests. It can be observed that both formulations are quite conservative. Additionally, neither of them accounts for the infill aspect ratio. Fig. 25 also shows that the two experimental curves are not significantly different in the range of low/intermediate IDRs, namely, when the IDR is normalized by means of IDR_{crack} the potential effect of the aspect ratio on the R factor seems to be not present.

Further formulations for the prediction of the OOP strength reduction due to IP damage were proposed by Morandi et al. [14] and by Verlato et al. [42] for URM thin and thick infills, respectively. The relationship proposed by Morandi et al. [14], which was derived based on Calvi and Bolognini [7]'s results, is more appropriate for the thickness of the infills tested herein. Such proposal is reported in Eq. (8) in its "stepwise" formulation and in Eq. (9) in its "linear" formulation. The results of the comparison of the experimental data with the predictions by Morandi et al. [14]'s formulations are reported in Fig. 26. Eqs. (8) and (9) represent an upper and a lower bound of the R factors registered for Calvi and Bolognini's tests up to an IP drift equal to 0.3%, which is roughly corresponding to the attainment of Damage Limitation Limit State. Actually, for very low drift values, the experimental R factors related to the specimens tested in the present study are bounded by the two curves proposed by Morandi et al. [14].

Table 10
Comparison of the experimental strength reduction factors with those predicted by Angel et al.'s formulation and by [41] formulation.

	IP_L-OOP	IP_M-OOP	IP_H-OOP			
IDR	0.15%	0.28%	0.51%			
IDR_{crack}	0.10%	0.09%	0.11%			
$IDR/2IDR_{crack}$	0.71	1.47	2.26			
R (exp.)	1.07	0.76	0.65			
R (pred. – Eq. (3))	0.73	0.51	0.36	Mean	median	CoV
exp/pred	1.47	1.48	1.81	1.59	1.48	12%
R (pred. – Eq. (4))	0.64	0.64	0.64	Mean	median	CoV
exp/pred	1.66	1.19	1.02	1.29	1.19	26%

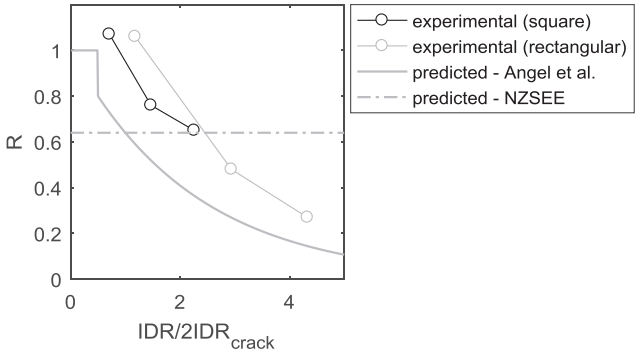

Fig. 25. Comparison of the experimental strength reduction factors with those predicted by Angel et al. [3]'s formulation and by NZSEE [41] formulation.

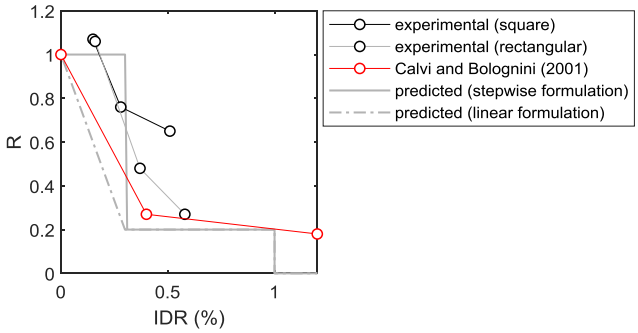

Fig. 26. Comparison of the experimental strength reduction factors with those predicted by Morandi et al. [14]'s formulations.

$$R = \begin{cases} 1.00 & IDR \leq 0.30\% \\ 0.20 & 0.30\% < IDR \leq 1.00\% \\ 0 & IDR > 1.00\% \end{cases} \quad (8)$$

$$R = \begin{cases} 1 - 2.67IDR & IDR \leq 0.30\% \\ 0.20 & 0.30\% < IDR \leq 1.00\% \\ 0 & IDR > 1.00\% \end{cases} \quad (9)$$

If R experimental values for rectangular and square infills are compared, a clear hierarchy among them is visible: R-values are higher in the case of square infills, especially in the range of intermediate-high IDRs values.

Another formulation to predict the OOP strength reduction R was proposed by Ricci et al. [24], as reported in Equation (10). Table 11 and Fig. 27 show the related predictions and the comparison with the experimental results presented herein, as well as with those associated with the nominally identical rectangular infills.

$$R = \min\{0.14(IDR)^{-1.12}; 1.00\} \quad (10)$$

Table 11 and Fig. 27 also show that Ricci et al. [24]'s formulation (which is derived from experimental results on infills similar to those tested in this study, but also on other results proposed in the literature) are quite good in predicting the effects of the IP/OOP interaction. A slight error exists on the safety-side for the square infills, mainly because this empirical formulation was derived based on a dataset

Table 11
Comparison of the experimental force reduction factors with those predicted by Ricci et al. [24]'s formulation.

	IP_L-OOP	IP_M-OOP	IP_H-OOP			
IDR	0.15%	0.28%	0.51%			
R (exp.)	1.07	0.76	0.65			
(pred. – Eq. (7))	1.00	0.58	0.30	mean	median	CoV
exp/pred	1.07	1.30	2.18	1.52	1.30	39%

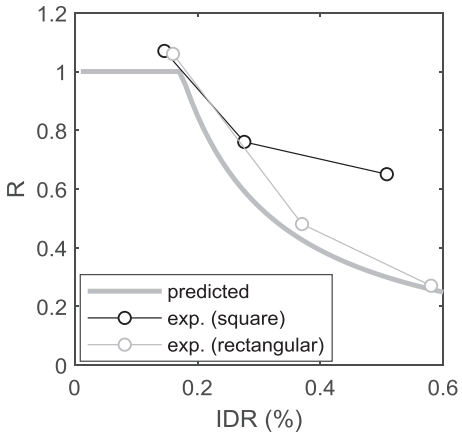

Fig. 27. Comparison of the experimental reduction due to the IP/OOP interaction of the OOP strength with those predicted by Ricci et al. [24]'s formulations.

constituted only by rectangular panels with quite high aspect ratios (ranging from 1.28 to 1.79).

Based on the above remarks, it is clear that the infill aspect ratio cannot be neglected in the evaluation of the IP/OOP interaction effects to avoid excessively safety-side results. As shown in Fig. 26 and Fig. 27, square panels exhibited, at equal IP drift demand, less detrimental effects of the IP displacement demand on the OOP performance with respect to rectangular panels for which concerns the OOP strength. Note that the lower entity of IP/OOP interaction effects for panels with lower aspect ratio was also assessed by means of numerical FEM analyses by Agnihotri et al. [13].

First, it is commonly recognised that the OOP strength reduction associated with IP/OOP interaction effects is due to the IP damage. Clearly, the entity of IP damage is strictly and mainly related to the drift demand. However, it is reasonable to suppose that also infill geometric and mechanical properties have some influence on the entity of damage: e.g., it is expected that less slender infills are characterized by lower damage than slender infills at identical IP drift demand, as highlighted also by Angel et al. [3] and discussed by Morandi et al. [43] based on Calvi and Bolognini [7] and on Morandi et al. [44] experimental tests on thin and thick masonry infills, respectively. About the IP damage, it is worth observing here the different damage states of rectangular and square panels at the end of the IP tests. Such damage states are reported in Fig. 28.

Fig. 28 shows that the square panels are significantly less damaged than the rectangular ones at each drift level, but especially at intermediate and intermediate-high displacement demand. In addition, Ricci et al. [24] noted that, at intermediate-high IP drift level, some hollow clay units were heavily damaged as their exterior tiles failed and overturned. This circumstance did not occur for square panels. Understanding the reason of the lower damage experienced by square panels and providing a mechanical demonstration for this issue is not straightforward. Additionally, as reported in Hak et al. [45], square infills should experience higher strain demand for the equivalent diagonal strut than rectangular infills at the same drift demand. Based on this finding, square infills are expected to be more damaged than rectangular infills at the same drift demand, contrary to the experimental outcomes described above. A possible explanation can be derived by analysing the experimental data, as reported below.

Fig. 29 shows the OOP central displacement of the specimens during the IP tests for the rectangular panels and for the square panels for the IP tests at the highest IP drift. The OOP displacement due to IP actions results higher for rectangular panel. It could be possible that the IP damage is, at least in part, due to OOP displacements produced by some sort of potential buckling phenomenon involving the diagonal struts forming in the infill thickness during IP tests. In this case, the higher damage for rectangular panels could be explained by a higher proneness to this sort of buckling phenomenon with respect to square infills. Clearly, further and ongoing studies are necessary to support and confirm this possible explanation of the experimental evidence.

6. Conclusions and future developments

Nowadays, it is commonly recognized that the analysis of the behaviour of the masonry infills under out-of-plane (OOP) and in-plane (IP) loading is paramount to correctly assess the seismic performance of reinforced concrete (RC) frames. A very important issue about this topic is certainly the IP/OOP interaction, namely the analysis of how the IP damage, which affect infills during earthquake, can influence their OOP behaviour and vice-versa. Some studies about this topic developed in last years; nevertheless, only a dozen of tests – all on rectangular walls – currently exist in the literature to experimentally explore this key issue.

This work first presented an experimental campaign carried out on square infill walls in RC frames to investigate about the OOP behaviour of the masonry infills and about the IP/OOP interaction. Then the influence of the infill aspect ratio (width (w)-to-height (h) ratio) on this interaction is investigated by means of the comparison between data presented herein and a companion experimental campaign previously performed and presented in Ricci et al. [24], nominally identical except that for the aspect ratio (w/h) of the infill (higher than the unit).

On the whole, four specimens have been tested under OOP monotonic loading. Three of them were first damaged under cyclic IP actions, with different extent; the remaining one (used as a reference) was tested under OOP loading only.

The reference IP-undamaged infill, named "OOP", is characterized, as expected, by the highest OOP strength (29.5 kN) and by the highest secant stiffness at first macro-cracking (9.62 kN/mm) and at peak load strength (4.93 kN/mm). The OOP strength of the specimen are quite well predicted by Ricci et al. [21]'s empirical formulation (with a relative percentage error, *e*, equal to −10%), together with Dawe and Seah [1]'s mechanical model if the (elastic) deformability of the surrounding RC frame is taken into account (e equal to −2%).

For what concerns the combined IP/OOP tests, it was observed that the OOP strength reduction due to IP damage was equal to −24% for the specimen damaged up to an IP drift equal to 0.28% and to −35% for the specimen damaged up to an IP drift equal to 0.51%. The specimen tested up to a very low IP drift equal to 0.15% exhibited a very small (+7%) increase of the OOP strength most likely due to experimental variability. Similar trends were observed for the other OOP response parameters (i.e., secant stiffness and force at first macro-cracking, secant stiffness at peak load).

Among the formulations proposed in the literature for the prediction of the IP/OOP interaction, only the one by Ricci et al. [24] showed quite good results in predicting this detrimental effect even if further improvement of this prediction could be obtained if the influence of some other parameters, e.g. the aspect ratio of the infills, was considered.

In fact, by comparing the results of the square panels with those obtained on the companion tests on rectangular specimens, nominally different from those presented herein only in terms of aspect ratio (equal to 1.28 instead of 1.00), it was observed that at roughly same drift demand, square and rectangular infills exhibit very different damage states, with the rectangular ones more damaged than square ones. This circumstance has some effects on the entity of the IP/OOP interaction, which is related more to the IP damage than to the IP drift. Namely, at drift demand equal to 0.28%, the square panel exhibited a strength reduction equal to −24% while the rectangular panel, at drift demand equal to 0.37% exhibited a strength reduction equal to −52%; at drift demand equal to 0.51%, the square panel exhibited a strength reduction equal to −35%, while the rectangular panel, at drift demand equal to 0.58%, exhibited a strength reduction equal to −73%.

This outcome (i.e., the more proneness of square infills to the IP/

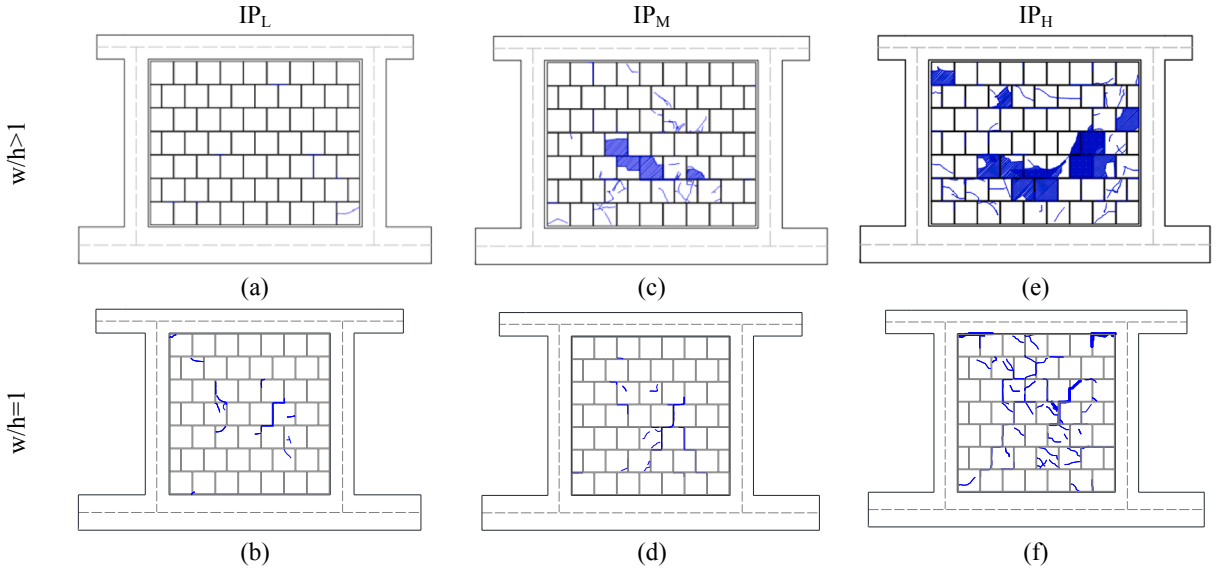

Fig. 28. Damage state at the end of IP tests for rectangular (a-c-e) and square panels (b-d-f) at low (a-b) intermediate (c-d) and intermediate-high (e-f) IP drift.

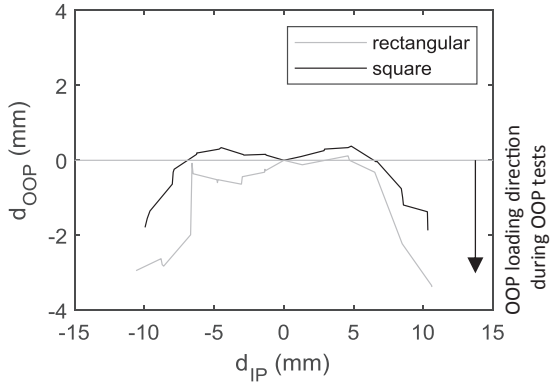

Fig. 29. Envelopes of the OOP central displacement for rectangular and square infills registered during the IP tests carried out up to the highest IP drift.

OOP interaction effects with respect to rectangular infills) was first observed by Agnihotri et al. [13] through numerical FEM analyses, but never confirmed by means of experimental tests. A possible explanation of this outcome and, in tune, of the higher damage of rectangular infills with respect to square infills, may be related to the OOP displacements – and the consequent damage – registered during IP tests (which are higher for rectangular infills than for square infills). However, it is worth to note that the present study is the first one experimentally investigating the IP/OOP interaction effects on square unreinforced masonry (URM) infills in RC frames and to compare them with equal rectangular infills. Future efforts are necessary to investigate the source of the influence of the aspect ratio on the IP/OOP interaction effects. Such efforts will be addressed to produce further experimental data on square URM infills, which are essential to adequately enrich the currently "totally-rectangular" database and update the predictive formulations proposed in the literature with the introduction of the infill aspect ratio among the predictive parameters. This should be done in order to account also for the above-demonstrated effects of the infill aspect ratio on the results of whichever formulation aimed at modelling the IP/OOP interaction effects and improve its predicting capacity.

Acknowledgements

This work was developed under the support of AXA Research Fund Post-Doctoral Grant "Advanced nonlinear modelling and performance assessment of masonry infills in RC buildings under seismic loads: the way forward to design or retrofitting strategies and reduction of losses", and ReLUIS-DPC 2014-2018 Linea CA -WP6 Tamponature funded by the Italian Department of Civil Protection (DPC). These supports are gratefully acknowledged.

References

[1] Dawe JL, Seah CK. Out-of-plane resistance of concrete masonry infilled panels. Can J Civ Eng 1989;16(6):854–64.
[2] Verderame GM, Ricci P, Di Domenico M. Experimental vs. theoretical out-of-plane seismic response of URM infill walls in RC frames. Struct Eng Mech 2019;69(6):677–91.
[3] Angel R, Abrams DP, Shapiro D, Uzarski J, Webster M. Behaviour of reinforced concrete frames with masonry infills. University of Illinois Engineering Experiment Station. College of Engineering. University of Illinois at Urbana-Champaign; 1994.
[4] Bashandy T, Rubiano NR, Klingner RE. Evaluation and analytical verification of infilled frame test data. Phil M. Ferguson Structural Engineering Laboratory, University of Texas at Austin; 1995.
[5] Flanagan RD, Bennett RM. Bidirectional behaviour of structural clay tile infilled frames. J Struct Eng 1999 1999;125.3:236–44.
[6] Flanagan RD, Bennett RM. Arching of masonry infilled frames: Comparison of analytical methods. Pract Period Struct Des Constr 1999;4.3:105–10.
[7] Calvi GM, Bolognini D. Seismic response of reinforced concrete frames infilled with weakly reinforced masonry panels. J Earthq Eng 2001;5(2):153–85.
[8] Pereira MFP, Pereira MFN, Ferreira JED, Lourenço PB. Behaviour of masonry infill panels in RC frames subjected to in plane and out of plane loads. 7th International Conference on Analytical Models and New Concepts in Concrete and Masonry Structures. 2011.
[9] Kadysiewski S, Mosalam KM. Modelling of unreinforced masonry infill walls considering in-plane and out-of-plane interaction. Pacific Earthq Eng Res Center 2009.
[10] Mosalam KM, Günay S. Progressive collapse analysis of reinforced concrete frames with unreinforced masonry infill walls considering in-plane/out-of-plane interaction. Earthq Spectra 2015;31(2):921–43.
[11] Longo F, Wiebe L, da Porto F, Modena C. Application of an in-plane/out-of-plane interaction model for URM infill walls to dynamic seismic analysis of RC frame buildings. Bull Earthq Eng 2018;16:6163–90.
[12] Varela-Rivera J, Moreno-Herrera J, Lopez-Gutierrez I, Fernandez-Baqueiro L. Out-of-plane strength of confined masonry walls. J Struct Eng 2012;138(11):1331–41.
[13] Agnihotri P, Singhal V, Rai DC. Effect of in-plane damage on out-of-plane strength of unreinforced masonry walls. Eng Struct 2013;57:1–11.
[14] Morandi P, Hak S, Magenes G. Simplified out-of-plane resistance verification for slender clay masonry infills in RC frames. In: Proceedings of the XV ANIDIS, L'Ingegneria Sismica in Italia, Padua, Italy, 2013.
[15] Guidi G, da Porto F, Dalla Benetta M, Verlato N, Modena C. Comportamento sperimentale nel piano e fuori piano di tamponamenti in muratura armata e rinforzata. In: Proceedings of the XV ANIDIS, L'Ingegneria Sismica in Italia, Padua, Italy, 2013, 30. [in Italian].
[16] Hak S, Morandi P, Magenes G. Out-of-plane experimental response of strong masonry infills. 2nd European Conference on Earthquake Engineering and Seismology. 2014.
[17] Furtado A, Rodrigues H, Arêde A, Varum H. Experimental evaluation of out-of-plane capacity of masonry infill walls. Eng Struct 2016;2016(111):48–63.

[18] Furtado A, Rodrigues H, Arêde A. Varum H 2016b. Simplified macro-model for infill masonry walls considering the out-of-plane behaviour. Earthq Eng Struct Dyn 2016;45(4):507–24.
[19] Oliaee M, Magenes G. In-plane out-of-plane interaction in the seismic response of masonry infills in RC frames. Brick and Block Masonry: In: Proceedings of the 16th International Brick and Block Masonry Conference, Padova, Italy, 26-30 June 2016.
[20] Di Trapani F, Shing PB, Cavaleri L. Macroelement model for in-plane and out-of-plane responses of masonry infills in frame structures. J Struct Eng 2018;144:04017198.
[21] Ricci P, Di Domenico M, Verderame GM. Empirical-based out-of-plane URM infill wall model accounting for the interaction with in-plane demand. Earthq Eng Struct Dynam 2018;47.3:802–27.
[22] Pasca M, Liberatore L, Masiani R. Reliability of analytical models for the prediction of out-of-plane capacity of masonry infills. Struct Eng Mech 2017;64(6):765–81. https://doi.org/10.12989/sem.2017.64.6.765.
[23] Di Domenico M, Ricci P, Verderame GM. Experimental assessment of the influence of boundary conditions on the out-of-plane response of unreinforced masonry infill walls. J Earthq Eng 2018. https://doi.org/10.1080/13632469.2018.1453411.
[24] Ricci P, Di Domenico M, Verderame GM. Experimental assessment of the in-plane/out-of-plane interaction in unreinforced masonry infill walls. Eng Struct 2018;2018(173):960–78.
[25] Ricci P, Di Domenico M, Verderame GM. Experimental investigation of the influence of slenderness ratio and of the in-plane/out-of-plane interaction on the out-of-plane strength of URM infill walls. Constr Build Mater 2018;2018(191):505–22. https://doi.org/10.1016/j.conbuildmat.2018.10.011.
[26] Preti M, Migliorati L, Giuriani E. Experimental testing of engineered masonry infill walls for post-earthquake structural damage control. Bull Earthq Eng 2015;13:2029–49.
[27] Mohyeddin A, Goldsworthy HM, Gad EF. FE modelling of RC frames with masonry infill panels under in-plane and out-of-plane loading. Eng Struct 2018;51:73–87.
[28] Morandi P, Milanesi R, Magenes G. Innovative solution for seismic-resistant masonry infills with sliding joints: in-plane experimental performance. Eng Struct 2018;2018(176):719–33.
[29] DM 2008. Decreto ministeriale 14 gennaio 2008 - Norme Tecniche per le Costruzioni NTC2008. Supplemento ordinario n. 30 Gazzetta Ufficiale 4 febbraio 2008, n 29. [in Italian].
[30] Petry S, Beyer K. Influence of boundary conditions and size effect on the drift capacity of URM walls. Eng Struct 2014;65:76–88. https://doi.org/10.1016/j.engstruct.2014.01.048.
[31] Frumento S, Magenes G, Morandi P, Calvi GM. Interpretation of experimental shear tests on clay brick masonry walls and evaluation of q-factors for seismic design. Research Report EUCENTRE 2009/02, IUSS Press, Pavia, Italy; 2009. ISBN: 978-88-6198-034-1.
[32] EN 206-1. Concrete. Part 1: specification, performance, production and conformity. European Committee for Standardization, Brussels; 2016.
[33] EN 10080. Steel for reinforcement of concrete – weldable reinforcing steel – general. European Committee for Standardization, Brussels; 2015.
[34] ASTM C109/C109M-16a, Standard Test Method for Compressive Strength of Hydraulic Cement Mortars, ASTM International, West Conshohocken, PA, 2016, www.astm.org.
[35] EN 1052-1. Methods of test for masonry. Part 1: determination of compressive strength. European Committee for Standardization, Brussels; 1999.
[36] ASTM E519-02, Standard Test Method for Diagonal Tension (Shear) in Masonry Assemblages, ASTM International, West Conshohocken, PA, 2002, www.astm.org.
[37] De Risi MT, Del Gaudio C, Ricci P, Verderame GM. In-plane behaviour and damage assessment of masonry infills with hollow clay bricks in RC frames. Eng Struct 2018;168:257–75.
[38] Del Gaudio C, De Risi MT, Ricci P, Verderame GM. Empirical drift-fragility functions and loss estimation for infills in reinforced concrete frames under seismic loading. Bull Earthq Eng 2019;17(3):1285–330.
[39] Cardone D, Perrone G. Developing fragility curves and loss functions for masonry infill walls. Earthq Struct 2015;9(1):257–79.
[40] ASCE/SEI 41-13. Seismic rehabilitation of existing buildings. Reston, VA: American Society of Civil Engineers; 2013.
[41] NZSEE 2017. New Zealand Society for Earthquake Engineering (NZSEE), Structural Engineering Society New Zealand Inc. (SESOC), New Zealand Geotechnical Society Inc., Ministry of Business, Innovation and Employment, Earthquake Commission. The Seismic Assessment of Existing Buildings (the Guidelines), Part C – Detailed Seismic Assessment, 2017. http://www.eq-assess.org.nz/.
[42] Verlato N, Guidi G, da Porto F. Experimental testing and numerical modelling of infill masonry walls subjected to in-plane damage. In: Proc of the Second European Conference on Earthquake Engineering and seismology, 25-29 August 2014, Istanbul, Turkey.
[43] Morandi P, Hak S, Magenes G. Performance-based interpretation of in-plane cyclic tests on RC frames with strong masonry infills. Eng Struct 2018;2018(156):503–21.
[44] Morandi P, Hak S, Magenes G. In-plane experimental response of strong masonry infills. Proceedings of the 9th International Masonry Conference. 2014.
[45] Hak S, Morandi P, Magenes G, Sullivan TJ. Damage control for clay masonry infills in the design of RC frame structures. J Earthq Eng 2012;16(Sup 1):1–35.